Electrical conductivity and crustal structure beneath the central Hellenides around the Gulf of Corinth (Greece) and their relationship with the seismotectonics

V. N. Pham, P. Bernard, D. Boyer, G. Chouliaras, J. L. Le Mouël, G. N. Stavrakakis

Geophys. J. Int. (2000) **142,** 948–969

Electrical conductivity and crustal structure beneath the central Hellenides around the Gulf of Corinth (Greece) and their relationship with the seismotectonics

V. N. Pham,[1] P. Bernard,[2] D. Boyer,[1] G. Chouliaras,[3] J. L. Le Mouël[1] and G. N. Stavrakakis[3]

[1] *Département de Géomagnétisme, IPGP,* 4 *Place Jussieu,* 75252 *Paris Cedex* 05, *France. E-mail: vnpham@ipgp.jussieu.fr*
[2] *Département de Sismologie, IPGP,* 4 *Place Jussieu,* 75252 *Paris Cedex* 05, *France*
[3] *National Observatory of Athens, Institute of Geodynamics,* PO Box 20048, 118–10 *Athens, Greece*

Accepted 2000 May 18. Received 2000 May 17; in original form 1999 June 8

SUMMARY

A deep magnetotelluric sounding (MTS) investigation in the western part of the Gulf of Corinth has revealed a complex electrical image of the crustal structure. The geotectonic structure of the Parnassos unit and the Transition zone in the central Hellenides, overthrusting the Pindos zone both towards the west and towards the south, has been clearly identified by its higher resistivity and its intrinsic anisotropy related to the N–S strike of the Hellenides range. Subsequent N–S extension of the Gulf introduced another heterogeneous anisotropy characteristic that corresponds to E–W-trending normal faults on both sides of the Gulf. The 2-D modelling of the MTS results reveals the existence of a relatively conductive layer about 4 km thick at a depth greater than 10 km in the middle crust. It corresponds to a ductile detachment zone suggested by microseismic and seismic studies (King *et al.* 1985; Rigo *et al.* 1996; Bernard *et al.* 1997a). It may be attributed to the phyllite series lying between the allochthonous Hellenic nappes and the autochthonous Plattenkalk basement. Towards the east, under the Pangalos peninsula, approaching the internal Hellenides, the detachment zone could root deeply into the lower crust.

Some strong local electrical anomalies are observed, reaching the conductive layer in the middle crust, such as that under the Mamousia fault and under the front of the overthrust of the Transition zone on the Pindos zone. Other anomalies affect only the shallower zones such as that beneath the Helike fault and in the Psaromita peninsula. These shallower anomalies provide complementary information to the study of spatial and temporal variations of the seismic anisotropy in relation to the short- and long-term tectonic activity of the Gulf (Bouin *et al.* 1996; Gamar *et al.* 1999).

Key words: crustal structure, electrical anisotropy, Gulf of Corinth, magnetotellurics.

1 INTRODUCTION

The Corinth rift in Greece, about 120 km long in a WNW–ESE direction with a mean width of about 20 km, is one of the most active tectonic areas of the Mediterranean region. The rift is presently opening at 1–1.5 cm year^{-1} according to GPS measurements (Briole *et al.* 1999), corresponding to a strain rate of 10^{-6} per year. The instrumental and historical seismicity is very high: five earthquakes with magnitudes greater than 6 in the last 30 years, the last one being the $Ms = 6.2$ 1995 June 15 Aigion earthquake, and several destructive historical earthquakes with estimated magnitudes of the order of 7 (Papazachos & Papazachos 1997).

Seismic studies in the east Corinth graben (King *et al.* 1985) and in Kalamata, south Peloponnesus (Lyon-Caen *et al.* 1988), reveal that seismogenic faults dip at angles of $40^\circ - 50^\circ$ and extend downwards to the base of the seismogenic layer at a depth of 8–12 km. This confirms the estimate of Doutsos & Poulimenos (1992) that the major faults of the Corinth graben extend to a depth of about 10 km, inferring the presence of a large curved ramp and a low-angle detachment fault in the upper crust. Melis *et al.* (1989) and King *et al.* (1985) speculated that the normal faults dipping north root on a north-dipping low-angle plane at 10–15 km depth. Rigo *et al.* (1996) showed that the microseismicity in the western part of the Gulf is mainly located at depths between 6 and 11 km, again suggesting

the existence of a detachment zone at a depth of around 10 km under the seismogenic layer. The geometry of the detachment would be that of a normal fault dipping 15° (±10°) northward.

A multidisciplinary study of the 1995 June 15 Aigion earthquake showed that the rupture nucleated at a depth of 10 km, 15 km NNE of the damaged city of Aigion and propagated southwards on a north-dipping low-angle (33°) offshore normal fault. This unusual low-angle normal fault may have been favoured by a low-friction, high-pore-pressure fault zone or, alternatively, by a rotation of the stress directions due to the possible dip towards the south of the mid-crustal ductile layer (Bernard *et al.* 1997a).

Detailed studies of the shallow crust anisotropy with shear wave splitting observations from local earthquakes led Bouin *et al.* (1996) and Bernard *et al.* (1997b) to show the existence of cracks predominantly oriented perpendicular to the regional extensional stress field. The extensional stress field was independently revealed by GPS measurements and by some specific orientations of neighbouring faults.

Despite these numerous recent seismic studies, the deep crustal structure of the Gulf remains widely unknown, as do its anisotropy characteristics. In order to acquire additional information on the deep structure and the anisotropy characteristics of the crust around the Gulf, the Institut de Physique du Globe de Paris (IPGP) and the Institute of Geodynamics of the National Observatory of Athens (NOA) have conducted, since 1995, several campaigns of broad-band magnetotelluric (MT) measurements in the western part of the Gulf (Fig. 1), allowing the electrical properties of the crust from the subsurface to its base to be studied. Preliminary MT results are given in Pham *et al.* (1996) and Chouliaras *et al.* (1997). In this paper, more extensive results are presented and discussed in relation to the seismotectonics of the Gulf, giving new insights into some characteristics of the seismicity distribution of the rift and the present strain rate as indicated by the geodesy.

2 TECTONIC AND GEOLOGICAL SETTING

The Gulf is an asymmetric graben formed since the Miocene, with a subsiding northern coast and a rising southern coast. This has resulted in the uplift of thick Plio-Quaternary deposits to the south and the cropping out of the bedrock on the northern coast (Ori 1989). The major active normal faults, located along the southern coast, are organized *en echelon* and have an average strike of N90°−105°E (see Fig. 1) and a northward dip of about 50° near the surface (Armijo *et al.* 1996). On the northern side, only small, less connected normal faults are identified.

The geological structure around the Gulf consists of a west-verging stack of flat-lying nappes belonging to the Hellenides, which correspond to a series of parallel isopic zones striking in a general NNW–SSE direction (Aubouin 1965; Jacobshagen *et al.* 1978b).

Fig. 2 shows a schematic E–W section across continental Greece on the north side of the Gulf, adapted from Jacobshagen *et al.* (1978a). At the bottom, the lowermost Plattenkalk series is believed to be the eastern continuation of the pre-Apulian zone and therefore should be autochthonous. The second tectonic level corresponds to the west Hellenic nappe system, which is composed of two units: the lower is the Phyllite series and the upper comprises the Ionian and Gavrovo–Tripolitza zones. Another tectonic level, the central Hellenic nappe system, comprises the Pindos nappe and the Parnassos unit. The Parnassos unit is a small platform composed of neritic

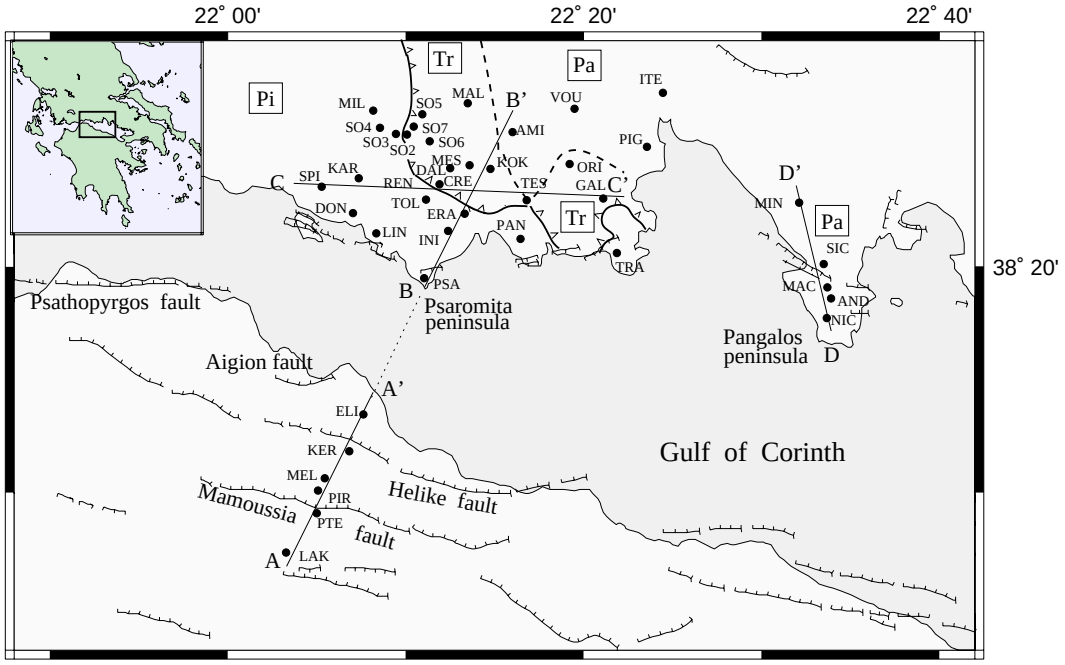

Figure 1. Inset shows the position of the study area. Location of the broad-band MTS stations on a simplified tectonic map showing normal faults from Armijo *et al.* (1996) and isopic zones, overthrust (heavy solid curve) and upthrust (heavy dashed curve), from the 1:50 000 geological map of Greece (Pi: Pindos zone; Tr: Transition zone; Pa: Parnassos zone). Thick lines indicate the locations of the profiles interpreted in Section 6. Figs 1 and 18 can be viewed in colour in the online version of the journal (www.blackwell-synergy.com).

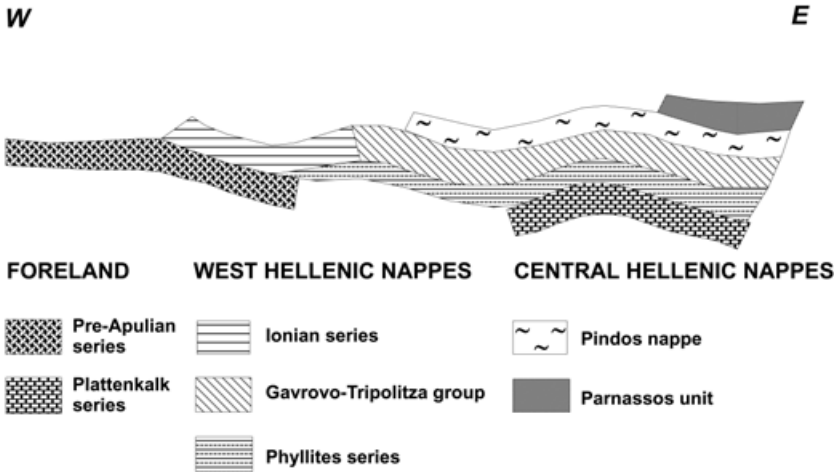

Figure 2. Schematic E–W geological cross-section through the nappe sequence on the northern side of the Corinth Gulf adapted from Jacobshagen *et al.* (1978a).

carbonates of Upper Triassic to Late Cretaceous age and several bauxite intercalations. In continental Greece, this unit, moderately folded, overrides the Pindos zone as a nappe (Jacobshagen *et al.* 1978b).

Each of these nappes consists of a competent series of Mesozoic carbonates, 2–3 km thick, and a thin, incompetent cover of flysch, with a maximum thickness of about 1.5 km (Doutsos & Poulimenos 1992). Aubouin *et al.* (1962) have evaluated the minimum thickness of each unit, as follows: Parnassos—2700 m; Pindos—3500 m; Gavrovo–Tripolitza—2300 m and Ionian—3100 m. These units were deformed and folded during the Tertiary E–W compression phase. After Middle Miocene nappe movement, the whole area became involved in general uplift and N–S extension (Doutsos & Poulimenos 1992). This is consistent with the overall Corinth rift structure, which is outlined by a prominent topographic depression trending ESE–WNW across the NNW–SSE-trending fabric of the Hellenic mountain belt (Armijo *et al.* 1996). The large normal faults that bound the rift cut the folded and thrust tectonic units of the Hellenides, resulting in a set of nearly perpendicular structures.

The study area is located in the western part of the Gulf, corresponding to the central Hellenic nappe system—the Pindos zone to the west and the Parnassos zone to the east. However, Aubouin (1965) has identified an ultra-Pindic subzone that is considered as a 'Transition zone' between the Pindos and Parnassos zones on the 1:50 000 geological map of Greece (see Fig. 3). According to this map, the Transition and Parnassos zones do not continue across the Gulf following the general trend of the Hellenides, but curve sinuously towards an E–W direction. The Transition zone overthrusts the Pindos zone to the west and to the south, and is separated from the Parnassos zone by an upthrust. The Parnassos unit constitutes a particular geotectonic structure in the frame of the Hellenides range and the Corinth rift. It has a specific electrical signature, as discussed below.

3 MAGNETOTELLURIC INVESTIGATION

The magnetotelluric (MT) method is a geophysical technique used to image the subsurface electrical conductivity (Cagniard

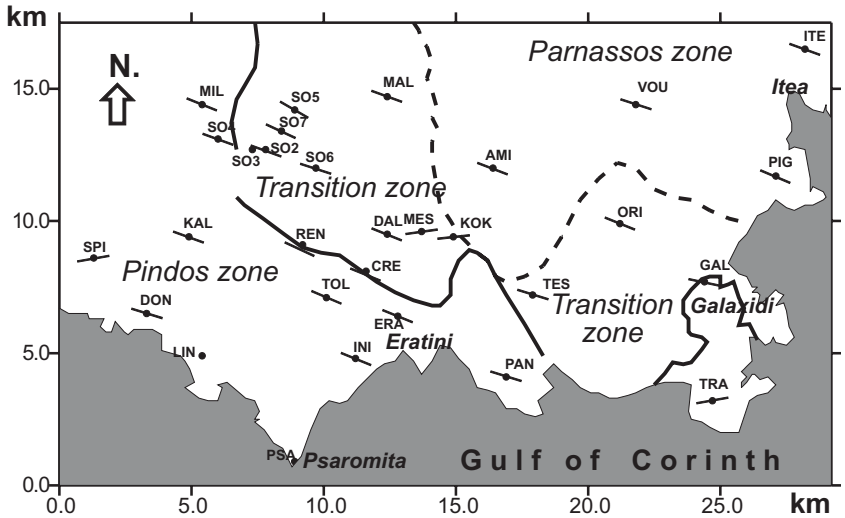

Figure 3. Details of the simplified tectonic map of the northern side of the Gulf in the study area (same captions as Fig. 1). Segments centred at each station represent one principal direction trending approximately E–W, the other being orthogonal.

1953; Vozoff 1991). Using as a source the Earth's natural electromagnetic field, whose range of periods is very broad, the investigation depth of the MT method can reach several tens of kilometres for longer periods, depending on the resistivity of the rocks. Because of the well-known phenomenon of the 'skin effect' (Cagniard 1953; Keller & Frischknecht 1966), the penetration depth of the electromagnetic field increases with period and resistivity. The technique used in this study is magnetotelluric sounding (MTS), which consists of observing the natural electromagnetic signals along two orthogonal directions and in a very broad band of frequencies, from 10^{-3} to 10^{3} Hz, covering six decades. One can then perform a tensor analysis of the data, which yields the variation of the apparent resistivity, ρ_a, with period, T (MT sounding curve), along two orthogonal principal directions corresponding to the two principal directions of the electrical anisotropy (see e.g. Pham *et al*. 1990; Vozoff 1991).

Since 1995, 40 MTS stations have been occupied in the western part of the Gulf of Corinth; most of them (34) are located on the northern side of the Gulf, with six on the southern side along a SSW–NNE profile (see Fig. 1).

4 PRINCIPAL DIRECTIONS AND ELECTRICAL ANISOTROPY

The results of tensor analysis show different electrical anisotropy characteristics, from low anisotropy (quasi-isotropic) to strong anisotropy along two principal directions. One of the principal directions of all stations coherently trends approximately E–W; it is represented in Fig. 3 by solid segments centred at each station on the northern side of the Gulf. The other, not shown here, is orthogonal, thus trending approximately N–S. The directions in Fig. 3 correspond to the period range 1–10 s; they vary by about $\pm 10^{\circ}$ in the entire frequency range ($10^{-3}-10^{3}$ Hz). The absence of a direction segment in the figure indicates weakly anisotropic behaviour (stations LIN and PSA).

The E–W direction of anisotropy is consistent with the general direction of the Corinth rift, and its orthogonal N–S direction is consistent with the general N–S trend of the isopic zones of the central Hellenides in the study area (Fig. 3). The principal directions obtained from the MT data confirm the set of nearly perpendicular structures resulting from the superposition of the past Hellenides tectonics and the present

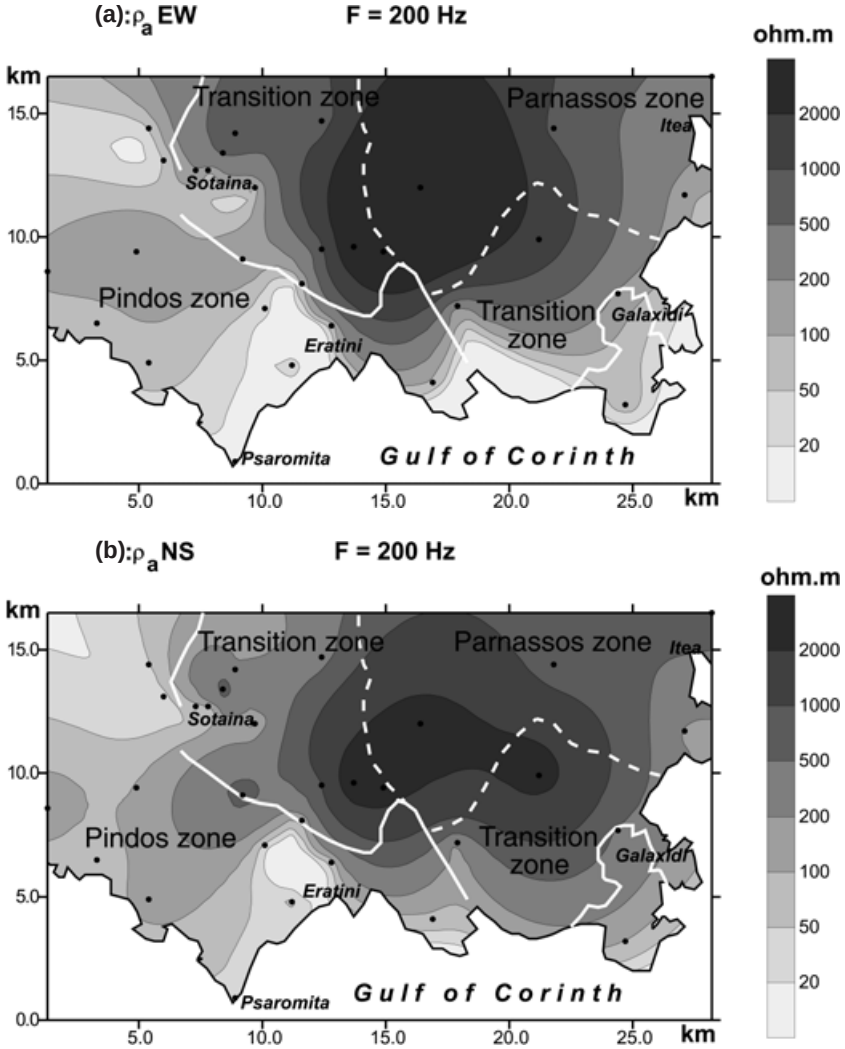

Figure 4. Apparent resistivity maps on the northern side of the Gulf (same location as Fig. 3) for frequency $F=200$ Hz for the two principal directions. (a) ρ_aEW; (b) ρ_aNS.

Corinth rift tectonics. However, it is not easy to distinguish the influence of each structure on the apparent electrical anisotropy, which has two different origins. The first is the 'intrinsic anisotropy' (Keller & Frischknecht 1966) of the rock fabric such as the layering of the sedimentary folded nappes (macroanisotropy), the existence of sets of parallel cracks, the schistosity and foliation of the metamorphic rocks, and the mineral and crenulation lineations of the compressed rocks (microanisotropy). The two principal directions of an intrinsic anisotropy are well defined: along the direction parallel to the layering, the cracks, the schistosity, the foliation and the lineation, the average electrical resistivity (longitudinal resistivity, ρ_l) is lower than along the perpendicular direction (transverse resistivity, ρ_t), $\rho_l < \rho_t$. Another origin of the apparent electrical anisotropy is the heterogeneity of the structure. The most simple case is the case of 2-D structure; MT analysis gives two principal directions, parallel (or longitudinal) and perpendicular (or transverse) to the strike of the structure. The corresponding anisotropy characteristics are more complicated, depending on the shape and on the depth of the structure and can be inferred only by numerical 2-D modelling (Doucet & Pham 1984; Vozoff 1991).

5 APPARENT RESISTIVITY MAPS

As explained above, tensor MT processing provides, for each frequency, two apparent resistivities, ρ_aEW and ρ_aNS, that correspond, respectively, to the two principal directions trending in the present study approximately E–W (Fig. 3) and N–S. A contour mapping of these apparent resistivities allows one to describe the spatial characteristics of the electrical conductivity distribution and its anisotropy. We have in fact a kind of tomography, since the different frequencies correspond to different penetration depths. However, the apparent

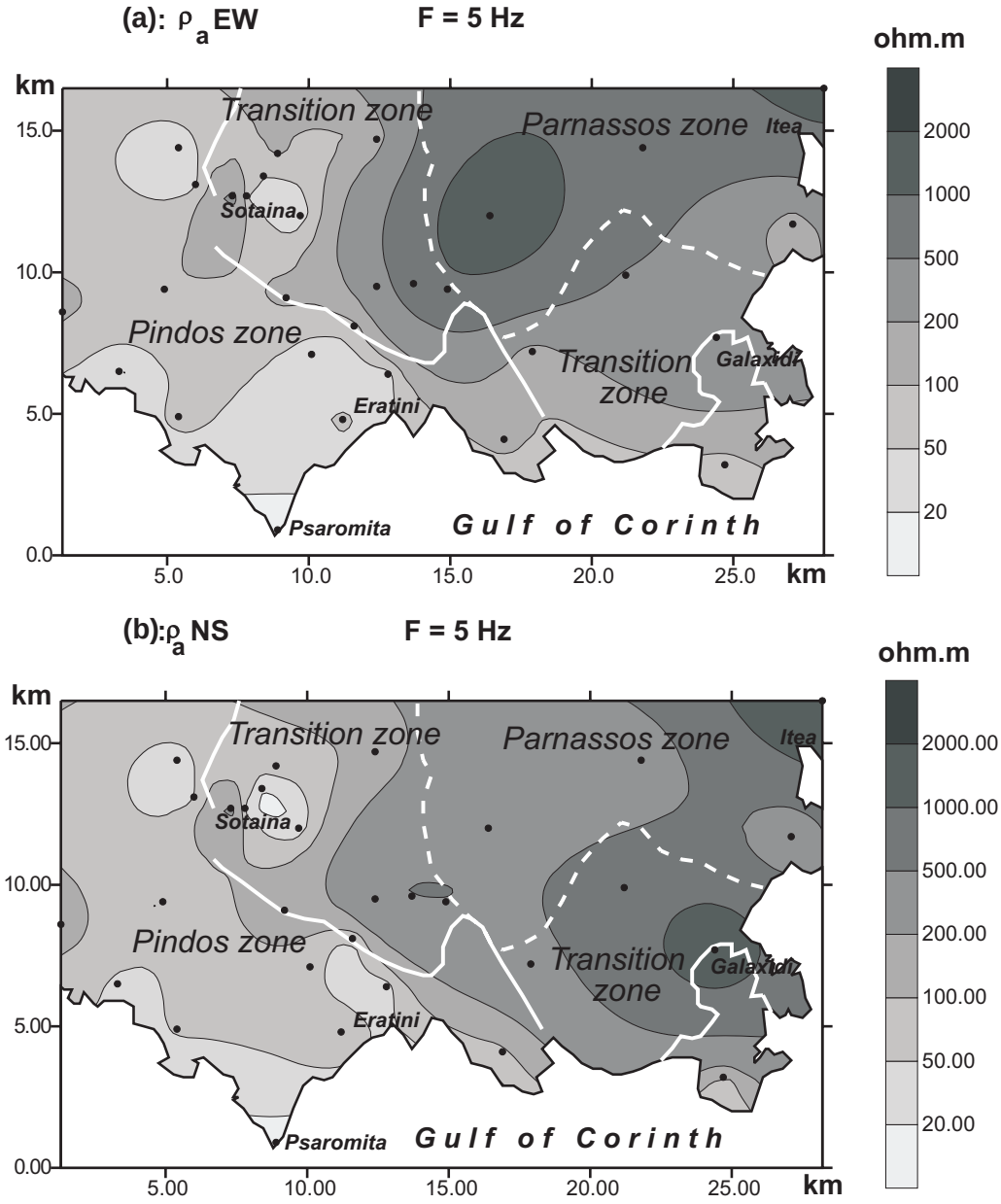

Figure 5. Same as Fig. 4 for frequency $F = 5$ Hz.

resistivity map does not correspond to a well-defined depth since the penetration depth also depends on the resistivity. Rather, it represents a smoothed electrical image of a wide zone. Because of the sparse distribution of the sites, only large electrical structures are discussed hereafter, except for the Sotaina region, where the density of the stations is higher.

Figs 4(a) and (b) show the apparent resistivity maps (ρ_aEW and ρ_aNS) on the north side of the Gulf for frequency $F=200$ Hz whose penetration depth is about a few hundreds metres (relatively shallow zone) for a resistivity of about 10–100 Ωm. We clearly observe the existence of a very resistive zone ($\rho_a > 2000$ Ωm) located in the Parnassos zone, which is composed principally of resistive neritic carbonate, bordered to the west and the SW by the more conductive Pindos zone, which contains thicker flysch series. The Transition zone shows intermediate apparent resistivities. The anisotropy characteristics can also be observed on the maps of apparent resistivity. In the southern part of the maps, ρ_aEW is lower than ρ_aNS, confirming the predominant influence of the rift on the electrical anisotropy in the shallower zone due to the E–W-striking normal faulting and fluid-filled cracks. In the northern part, the anisotropy is less important, but ρ_aNS is lower than ρ_aEW, showing the dominance of the signature of the central Hellenides tectonics.

Figs 5(a) and (b) show the same apparent resistivity maps for the frequency $F=5$ Hz, which corresponds to a penetration depth of a few kilometres (intermediate depth zone). The same comments as above apply for these maps. The most interesting feature is the appearance of a local conductive anomaly in the neighbourhood of Sotaina village, which is located on the western border of the Transition zone.

Figs 6(a) and (b) show maps corresponding to the period $T=50$ s, the penetration depth of which can reach a few tens of kilometres. The correlation between the spatial variation of the apparent resistivity and the isopic zones is not clear. The Sotaina anomaly remains well defined and could be connected with a major change in strike of the overthrust of the Transition zone over the Pindos zone (see Section 8 and Appendix A).

6 QUANTITATIVE MODELLING

The apparent resistivity maps give a qualitative image of the electrical properties of the crust. More quantitative results can be obtained by numerical modelling along some specific profiles. There is no unique solution for the inversion of the MT results as for any of the potential field methods. We can only propose a best-fit model from a large trial set, taking into

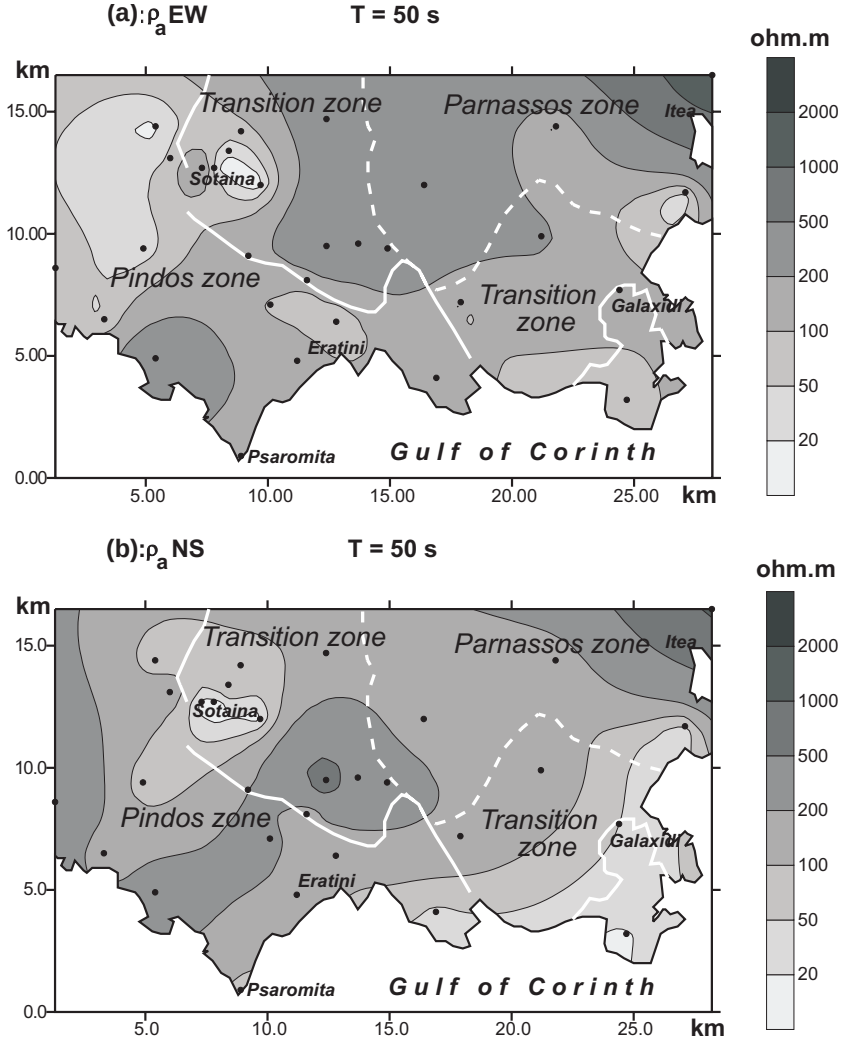

Figure 6. Same Fig. 4 for period $T=50$ s.

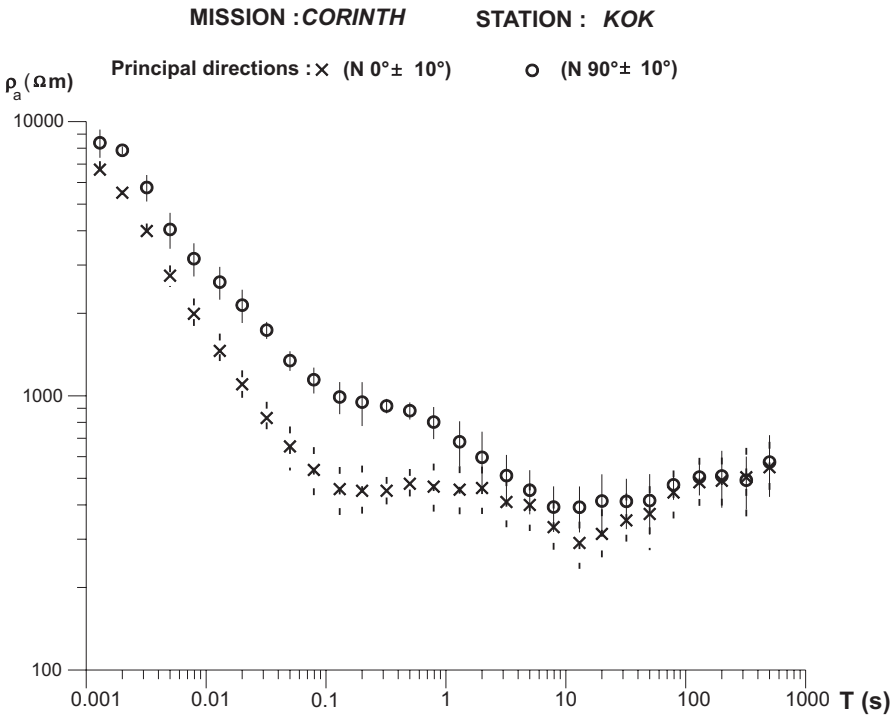

Figure 7. Example of MT sounding curve along two principal directions at station KOK located in the western part of the study area. Solid and dashed vertical bars represent the standard deviation of experimental results.

account the geological information and the seismotectonic environment. However, it is well known that the MT method gives the best resolution for the localization of the conductive zones (Vozoff 1991), which are representative of tectonometamorphic zones, fractured zones and their fluid contents. As an example, Fig. 7 shows the MT sounding curve (ρ_a versus T) along two principal directions at station KOK located in the western part of the study area (Fig. 1). We clearly observe the existence of two conductive zones (minimum ρ_a) corresponding to short periods ($\sim$0.1 s) or the shallower zone and to long periods ($\sim$10 s) or the deeper zone. The latter can be interpreted as a conductive layer located in the middle crust ($\sim$9–13 km)

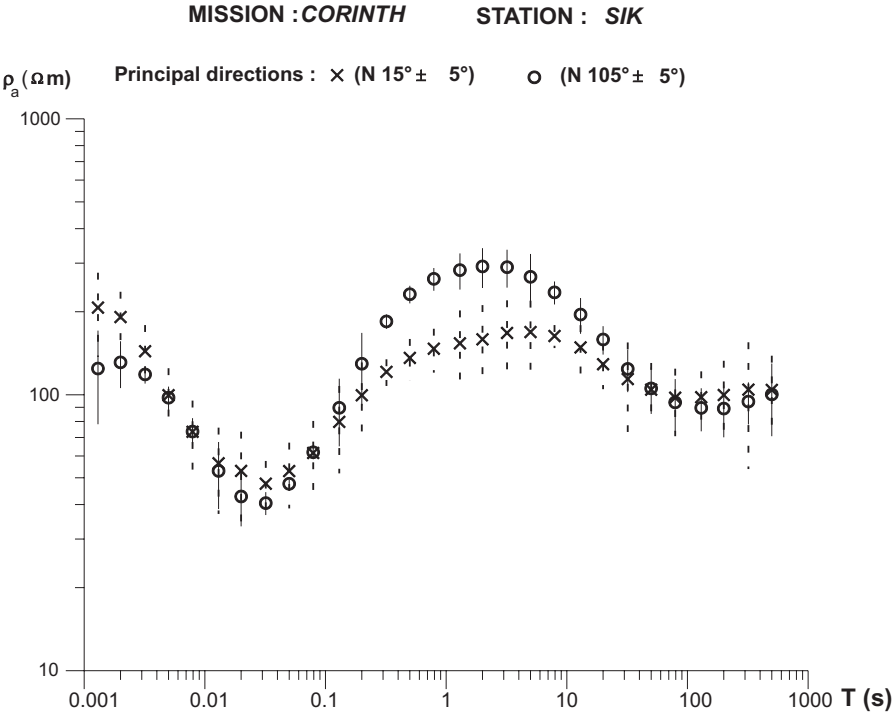

Figure 8. Example of MT sounding curve along two principal directions at station SIK located in the eastern part of the study area. Solid and dashed vertical bars represent the standard deviation of experimental results.

in the case of a 1-D model (see Fig. 15 and the discussion in Section 6.3). Another example is shown in Fig. 8 corresponding to station SIK located in the eastern part of the study area; the deep conductive zone ($T > 10$ s) can be interpreted as a conductive layer in the lower crust ($\sim$20–30 km) in the case of a 2-D model (see Fig. 17 and the discussion in Section 6.4). Of course, 2-D modelling is better constrained than 1-D modelling, taking into account not only several stations along a profile, but also, for each station, two polarization modes of the MT field: the *E*-polarization and the *H*-polarization, corresponding, respectively, to the electric (or telluric) field, *E*, and the magnetic field, *H*, parallel to the strike of the structure (Doucet & Pham 1984; Vozoff 1991). Therefore, the interpreted profile must be oriented perpendicular to the strike.

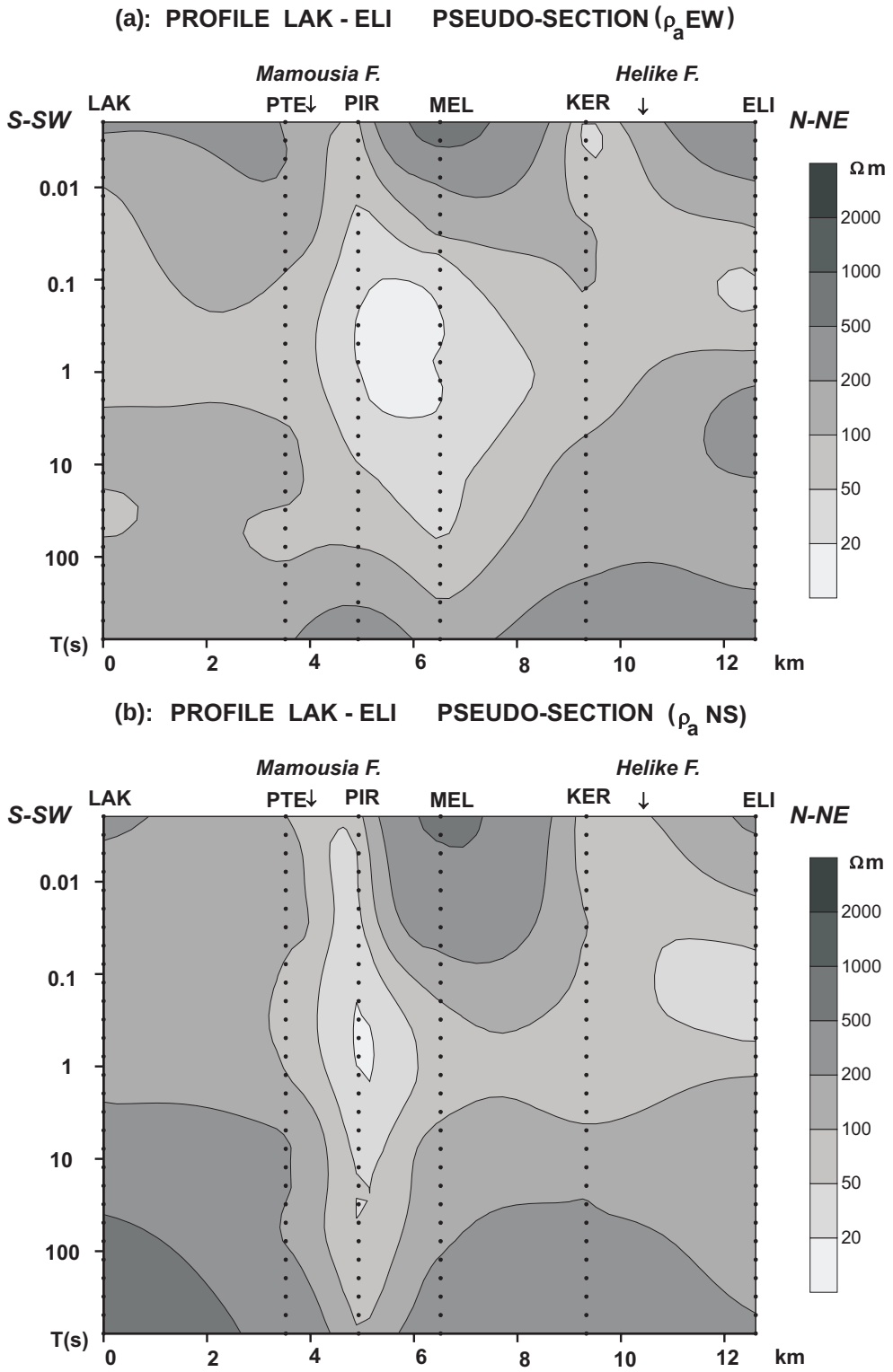

Figure 9. Pseudo-sections of the profile LAK-ELI (AA′ in Fig. 1). (a) ρ_aEW; (b) ρ_aNS.

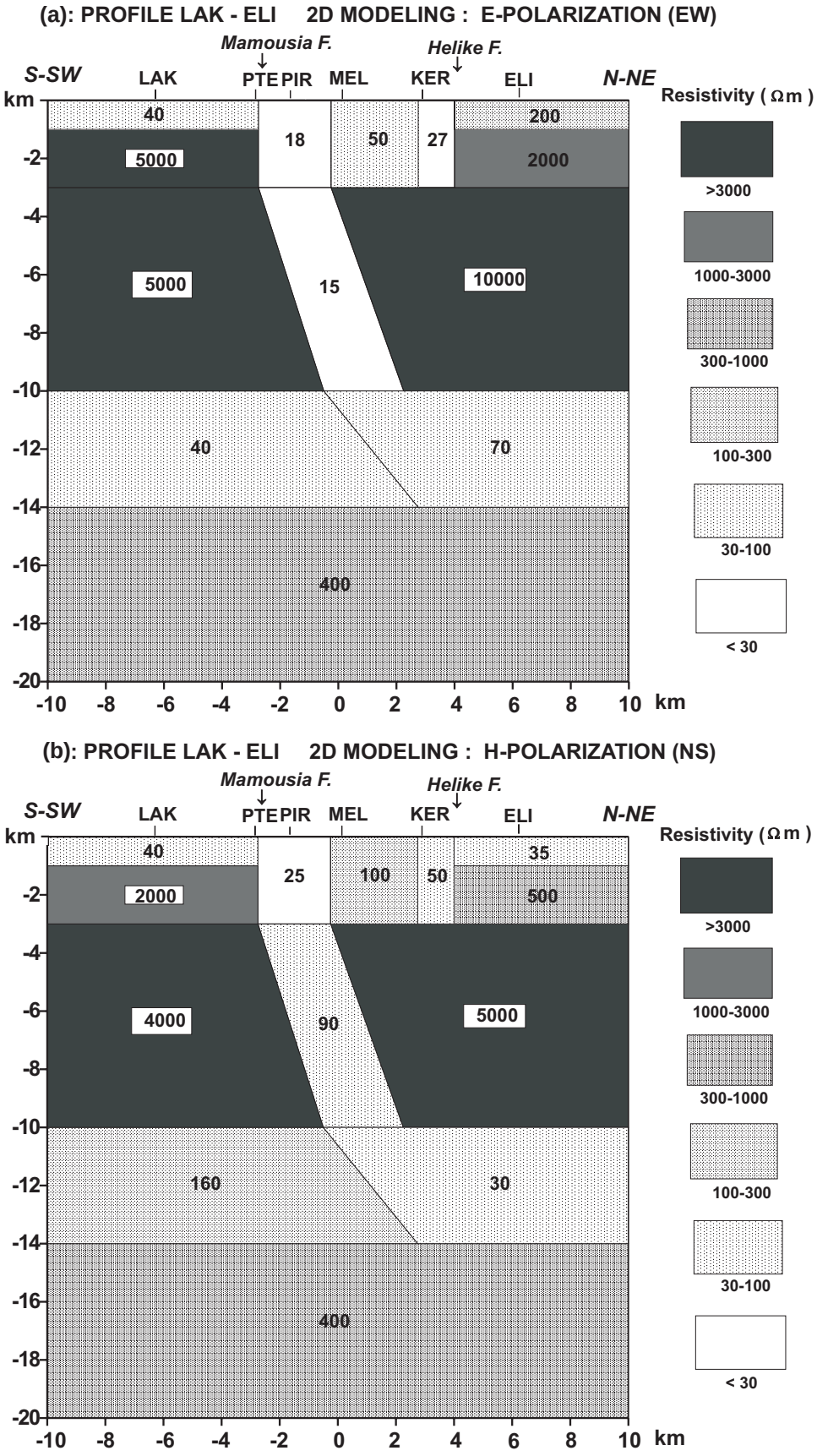

Figure 10. 2-D geoelectrical sections of the profile LAK-ELI. (a) *E*-polarization mode; (b) *H*-polarization mode.

6.1 Profile LAK-ELI

The LAK-ELI profile, about 12 km long in a SSW–NNE direction (profile AA′ in Fig. 1), located on the south side of the Gulf, is composed of six MTS stations. It crosses two main north-dipping normal faults, the Mamousia and Helike faults (Armijo *et al.* 1996).

A qualitative electrical image of the structure along the profile can be observed on the pseudo-section, which shows the variation of the apparent resistivity from short $T \sim 10^{-3}$ s (shallow zone) to long periods, $T \sim 10^{3}$ s (deep zone). The two pseudo-sections, corresponding, respectively, to ρ_aEW and ρ_aNS (Figs 9a and b), clearly show the existence of a large and deep conductive zone under the Mamousia fault; its form is suggestive of a north-dipping fault zone striking perpendicular to the profile. Under the Helike fault, only a small and shallow conductive zone is observed.

Figs 10(a) and (b) show a best-fit 2-D model. The theoretical results are compared with the experimental results in Figs 11(a) and (b), respectively, for two polarization modes and three frequencies: 1, 0.1 and 0.01 Hz. On the LAK-ELI profile, oriented approximately N–S, the *E*-polarization corresponds to ρ_aEW (Fig. 10a) and the *H*-polarization to ρ_aNS (Fig. 10b). The best-fit model can be obtained only by introducing electrically anisotropic blocks with the same geometrical constraint for both polarizations.

The 2-D model suggests the existence of a strong conductive zone under the Mamousia fault, about 2 km wide, E–W striking and N dipping, reaching 10 km depth. Its resistivity along the E–W direction is as low as 15 Ωm and can be explained by the presence of fluids in a fractured zone. Beneath the Helike fault, a small conductive block is limited to a depth of about 3 km.

The other striking result is the existence of a relatively conductive layer, about 4 km thick, below 10 km depth. The thickness is better constrained by 2-D modelling than by a preliminary 1-D interpretation (Pham *et al.* 1996). The upper crust above the conductive layer is very resistive (>4000 Ωm) and anisotropic; its intrinsic anisotropy, with the N–S resistivity lower than the E–W resistivity, can be related to Hellenides tectonics. The crust below the conductive layer is less resistive (~ 400 Ωm) and quasi-isotropic.

6.2 Profile PSA-AMI

The profile PSA-AMI is located on the northern side of the Gulf and is a continuation of the LAK-ELI profile. It is about 13 km long in a SSW–NNE direction (profile BB′ in Fig. 1). It crosses successively the overthrust of the Transition zone over the Pindos zone and the upthrust between the Transition zone and the Parnassos zone.

Figs 12(a) and (b) show pseudo-sections corresponding, respectively, to ρ_aEW and ρ_aNS. They reveal essentially two distinct electrical domains, conductive to the south of the overthrust and resistive to the north. The 2-D modelling (Figs 13a and b), using the same constraints as for the LAK-ELI profile

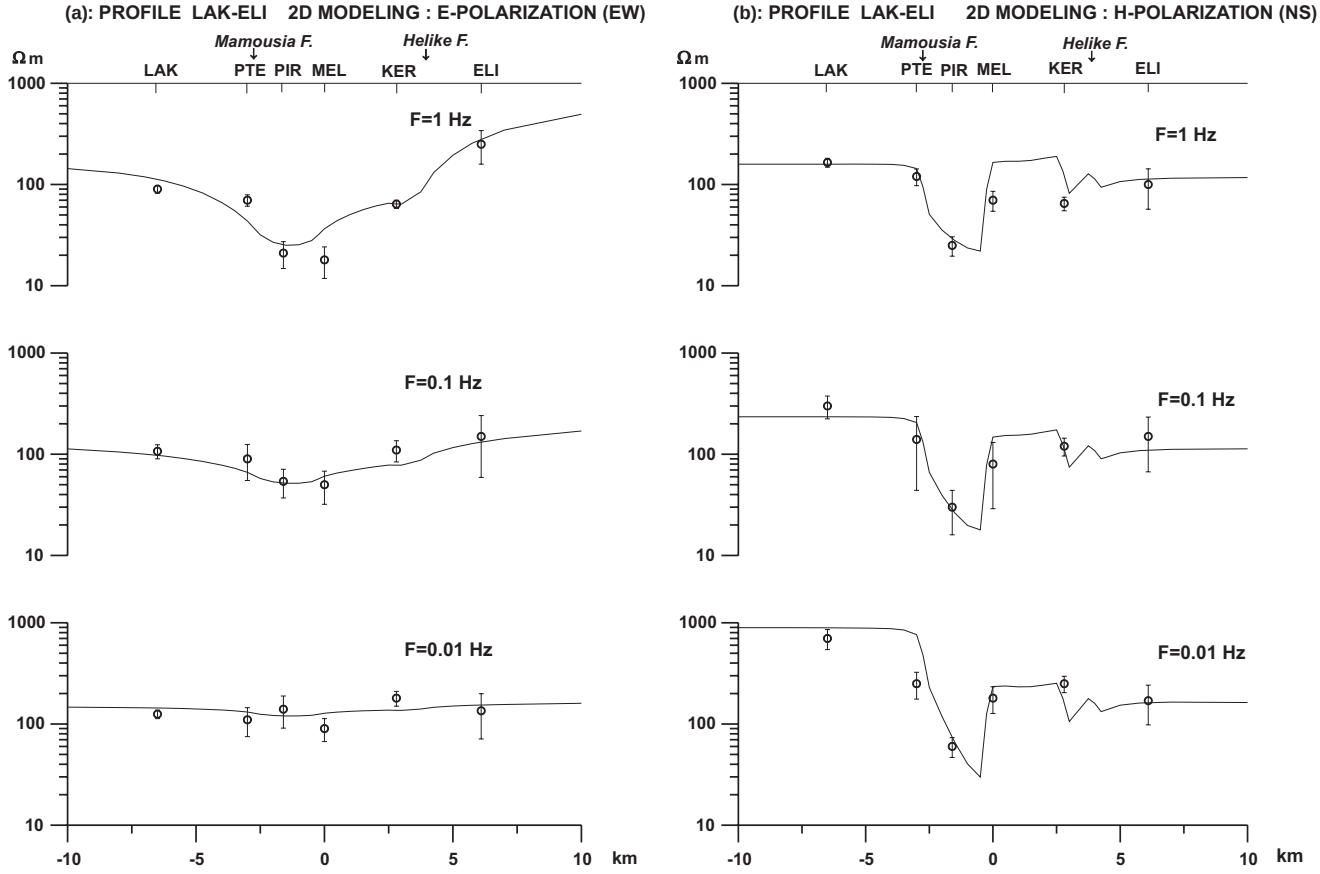

Figure 11. Comparison between experimental (white circles) and theoretical (solid curves) results obtained from 2-D modelling of the profile LAK-ELI for three frequencies: 1, 0.1 and 0.01 Hz. Vertical bars represent the standard deviation of the experimental results. (a) *E*-polarization mode; (b) *H*-polarization mode.

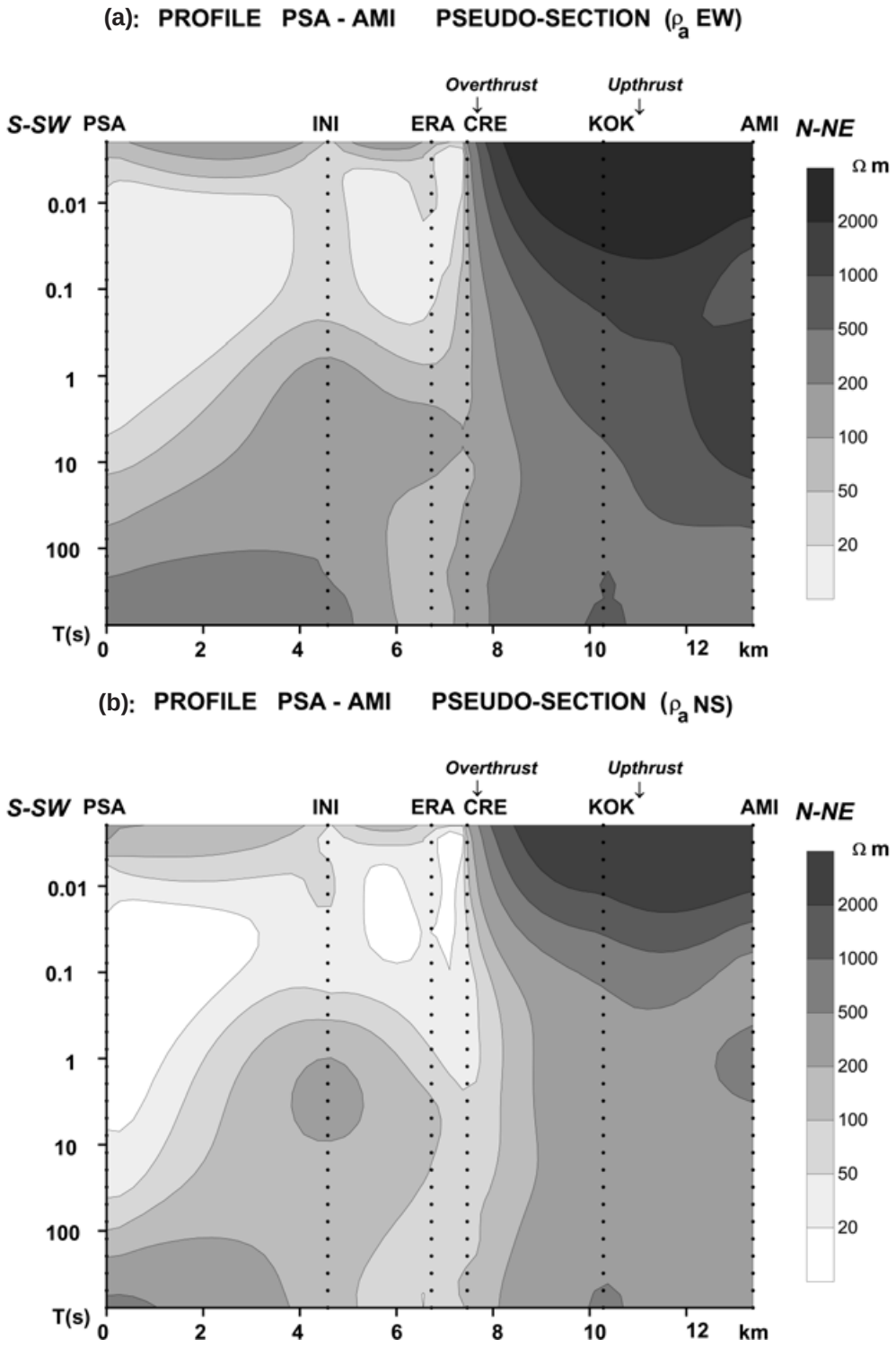

Figure 12. Pseudo-sections of the profile PSA-AMI (BB′ in Fig. 1). (a) ρ_aEW; (b) ρ_aNS.

(identical geometry for both polarizations and anisotropic blocks), shows the existence, under the overthrust, of a strong electrical discontinuity represented by a conductive zone of about 2 km width extending to about 10 km depth. Its resistivity along the E–W direction is as low as under the Mamousia fault ($\sim$15 Ωm) and confirms the presence of fluids in a fractured zone. This discontinuity seems to continue deeply into the crust. On the other hand, the upthrust between the Transition zone and the Parnassos zone is not associated with any strong resistivity contrast. The crust beneath both zones has the same electrical characteristics: it is very resistive and anisotropic, the most conductive direction being oriented N–S like the Hellenides strike.

South of the overthrust the upper crust in the Pindos zone is less resistive. A striking feature is the existence of a very conductive shallow layer ($\sim$8 Ωm) about 1–2 km thick in the neighbourhood of station PSA. A detailed study of seismic and electric anisotropy in the Psaromita peninsula confirms the

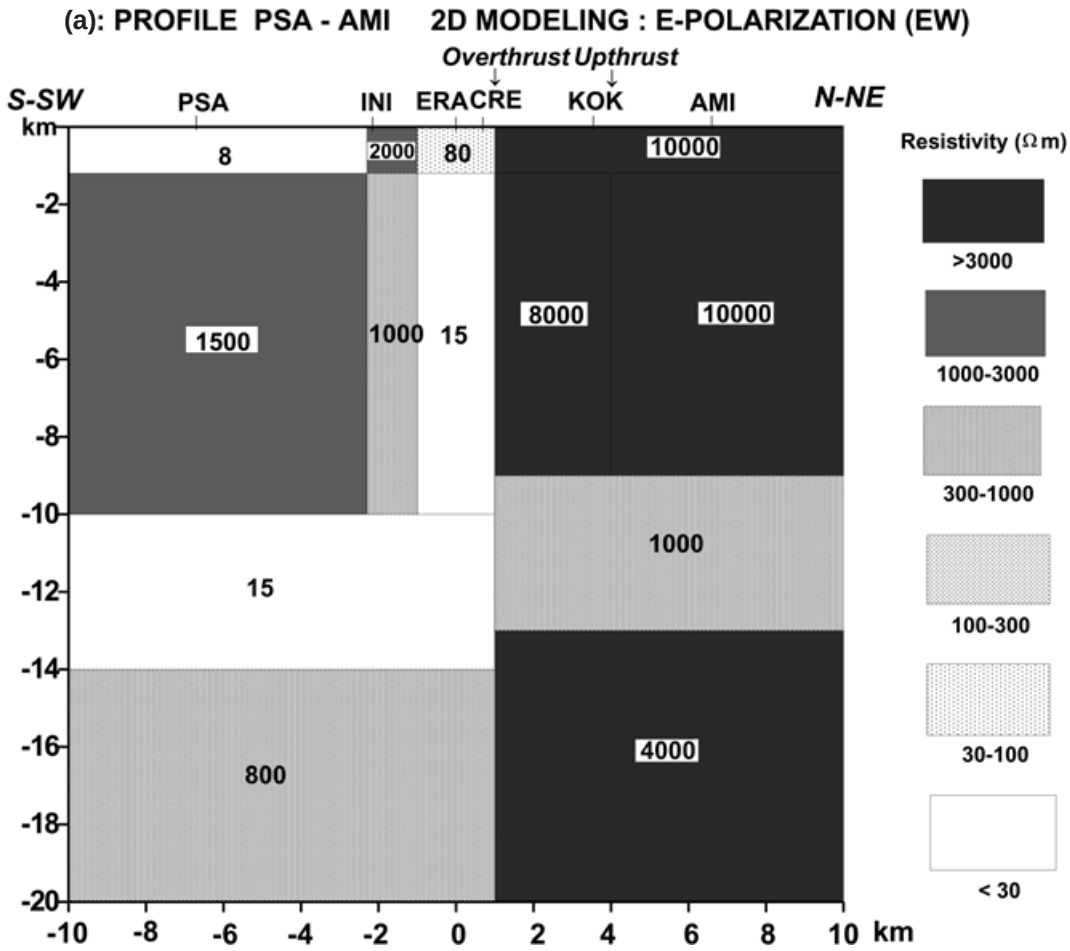

Figure 13. 2-D geoelectrical sections of the profile PSA-AMI. (a) *E*-polarization mode; (b) *H*-polarization mode.

presence of cracks in the shallower layer (1.5–2 km), oriented along the regional stress field of the Gulf and interpreted as being due to flexure related to the long-term activity of the normal faulting (Gamar *et al.* 1999).

The final interesting result observed on the PSA-AMI profile is again the existence of a relatively conductive layer below 9–10 km depth, which seems to be cut off or altered by the overthrust of the Transition zone over the Pindos zone.

6.3 Profile SPI-GAL

The SPI-GAL profile is located on the northern side of the Gulf, but its orientation is E–W, running along the southern border between the Transition zone and the Parnassos zone (profile CC′ in Fig. 1). It crosses obliquely the overthrust and the upthrust, so that it is not legitimate to interpret the corresponding MT results using a 2-D model. However, a simple 1-D model can provide some information about the deep structure. Figs 14(a) and (b) show the pseudo-sections corresponding, respectively, to ρ_aEW and ρ_aNS. These electrical images confirm the results observed on the PSA-AMI profile, that is, that the overthrust is associated with an electrical discontinuity between the resistive Transition and Parnassos zones to the east and the conductive Pindos zone to the west.

The simple 1-D model (Figs 15a and b) interpretation, using the same constraints as the former 2-D modelling (identical geometry, anisotropic layer), confirms again the electrical characteristics of the upper crust under both the Transition zone and the Parnassos zone: the resistivity is high and the anisotropy is consistent with the Hellenides strike. The resistivity is lower under the Pindos zone, with an exceptional conductive zone under station KAL, probably related to the front of the overthrust. Finally, the 1-D model shows the existence of the same relatively conductive layer below 9–10 km depth. Therefore, this layer displays regional extension under the study area.

6.4 Profile NIC-MIN

The NIC-MIN N–S profile is composed of five stations far away in the eastern part of the study area, in the Pangalos peninsula located south of Delfi (profile DD′ in Fig. 1). The profile crosses a fault zone that was mapped by Armijo *et al.* (1996) as a presently active small graben bordered by normal and antithetic faults (see Fig. 1). Aubouin (1965) and Jacobshagen *et al.* (1978b) identified this fault zone as an overthrust of the Parnassos zone over the Pindos zone, which is thus reactivated in the present N–S extension.

The pseudo-sections (Figs 16a and b) show an electrical image quite similar to the image of the PSA-AMI pseudo-sections: a resistive Parnassos zone to the north and a conductive Pindos zone to the south. The 2-D modelling (Figs 17a and b) confirms the existence of an anisotropic resistive upper crust under the Parnassos zone, the resistivity being lower along the N–S direction, as already observed on the other profiles. Under the Pindos zone on the south side of the overthrust, the structure of the whole upper crust is complicated and heterogeneous and its

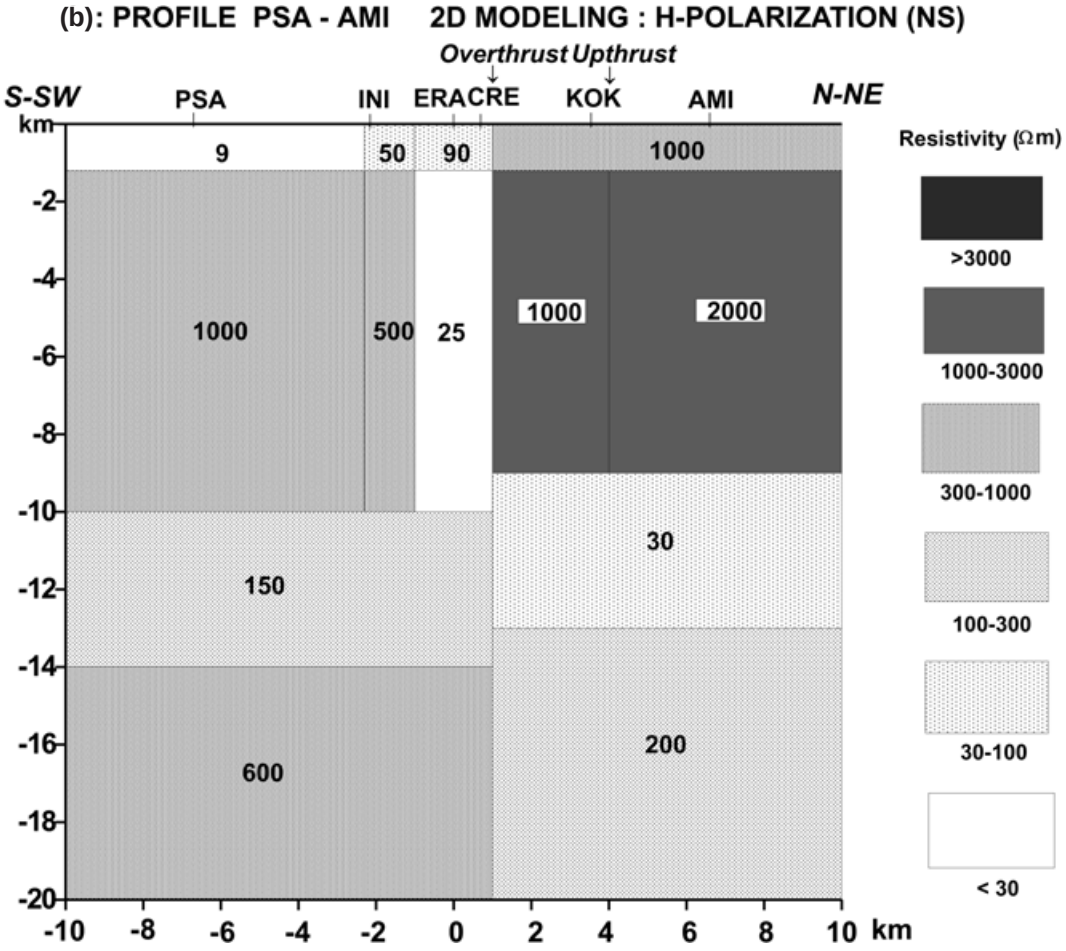

Figure 13. (*Continued.*)

resistivity is generally low (<100 Ωm). The southern part of the Pangalos peninsula appears to be very fractured at depths greater than under the Psaromita peninsula. These fractures and the associated anisotropy could be related to the extension of the Gulf and to the flexure of the Pangalos peninsula, which probably reactivated the overthrust in particular, forming a small graben at its front (see Fig. 1).

The other interesting feature of this profile is the absence of a relatively conductive layer in the middle crust (10–15 km), which was verified by numerous trial models. Its absence allows one to observe a deeper thick conductive zone (between 20 and 30 km), which is commonly encountered in the lower crust (Pham *et al*. 1990, 1998; Jones 1992). The bottom of this conductive zone can be identified as the Moho discontinuity; the depth of about 30 km is indeed consistent with the results of deep seismic sounding (Makris 1978), which gave crustal thicknesses of about 32 km below north Evia, 30 km below south Evia and 28 km below Mikonos island.

7 ON THE NATURE OF THE CONDUCTIVE LAYER IN THE MIDDLE CRUST

As mentioned in Section 1, several seismic studies in the Corinth rift suggest the existence of a detachment zone under the brittle seismogenic upper crust, corresponding to the transition to a ductile lower crust. However, the origin and nature of the ductile zone are poorly known. The study of the electrical properties of the crust by the MTS method confirms the existence of this ductile zone, which corresponds to a relatively conductive layer located below 9–10 km depth in the western part of the study area. This layer does not extend to the whole lower crust but constitutes a distinct layer in the middle crust, about 4 km thick, according to the best-fit 2-D model. Its high conductivity may be explained by the presence of fluids in a tectonometamorphic zone.

What is the nature of this conductive and ductile layer? According to Aubouin *et al*. (1963) and Doutsos & Poulimenos (1992), the three units, Parnassos, Pindos and Gavrovo–Tripolitza, have a minimum total thickness of about 8.5 km (see Section 2). Beneath these three units, Jacobshagen *et al*. (1978a) suggested the presence of the Phyllite series (see Fig. 2): 'It comprises preponderantly phyllites, chlorite schists, quartzites and meta-volcanites'. Jacobshagen *et al*. (1978a) concluded that 'the importance of the tectonic contact between the Phyllite series and the Plattenkalk sequence is without any doubt' and that the upper contact to the Gavrovo–Tripolitza unit is also of undoubted tectonic origin. The lithology of the Phyllite series and its palinspastic position (see Fig. 2) suggest that this unit is of tectonometamorphic origin. According to Jacobshagen *et al*. (1978b), the Pre-Apulian foreland and the Plattenkalk series may be regarded as being autochthonous, whereas the west-verging stack of flat-lying west and central Hellenic nappes may be regarded as being allochthonous. This suggests a large-scale

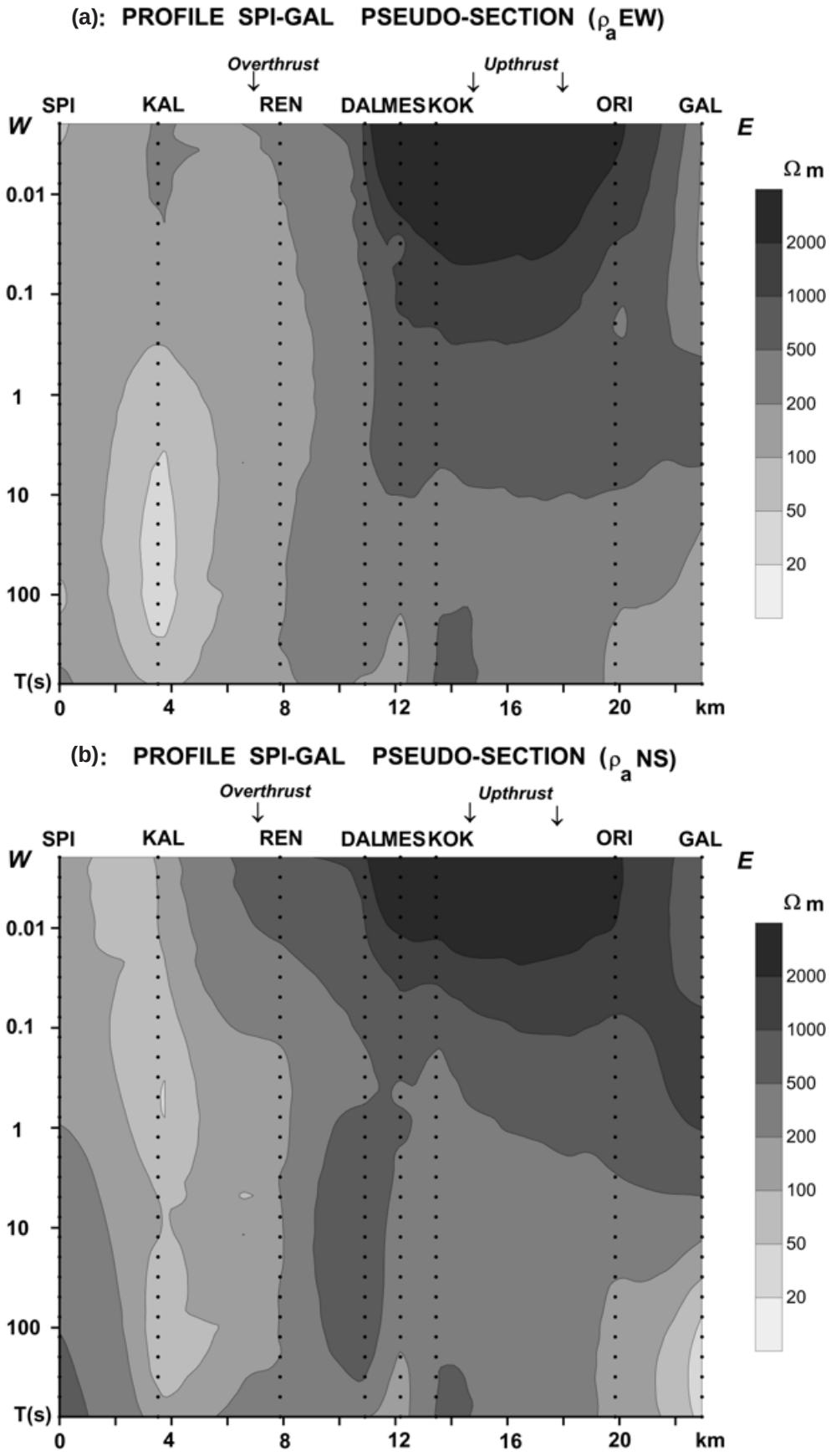

Figure 14. Pseudo-section of the profile SPI-GAL (CC′ in Fig. 1). (a) ρ_aEW; (b) ρ_aNS.

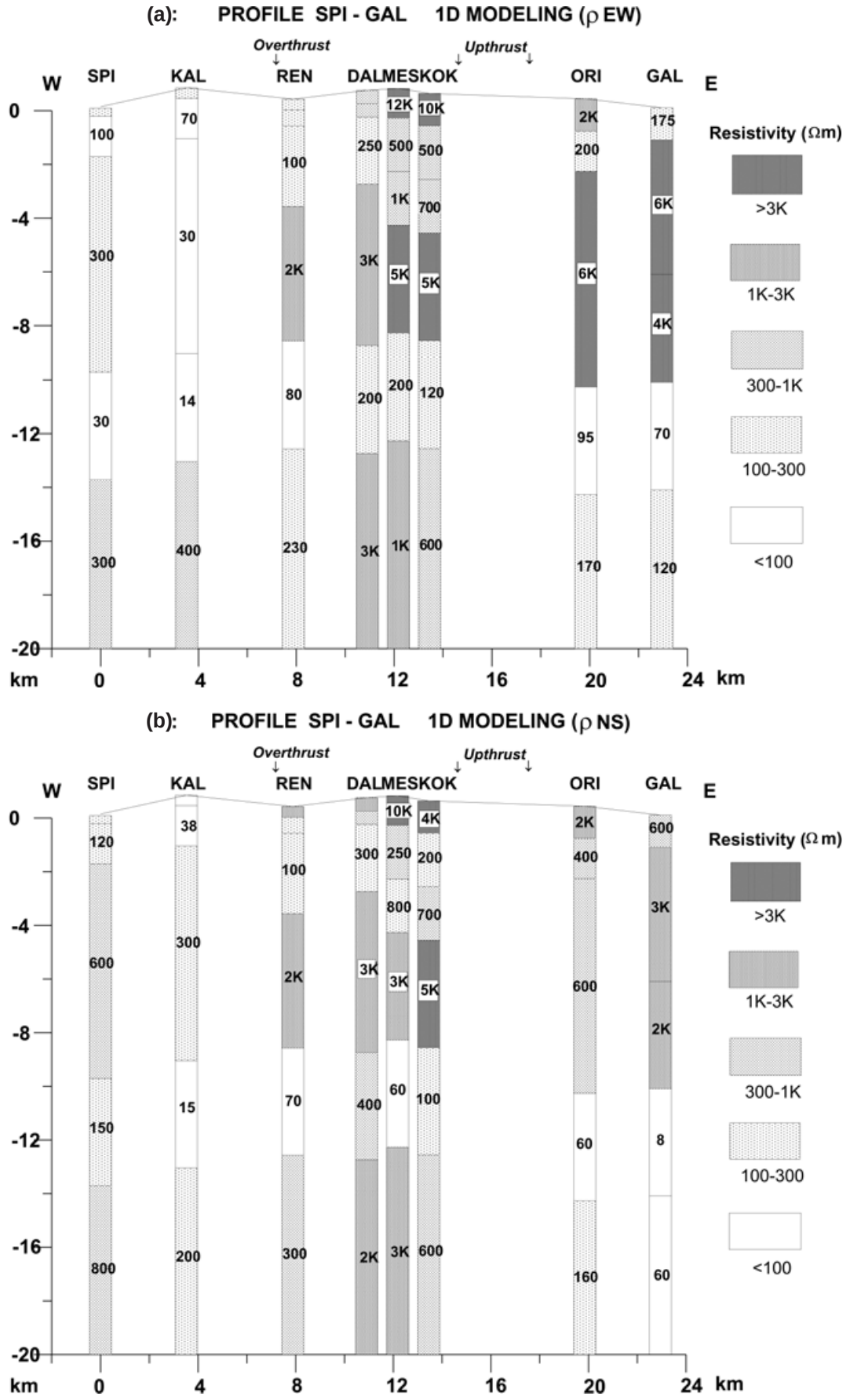

Figure 15. 1-D geoelectrical sections of the profile SPI-GAL. (a) ρ_aEW; (b) ρ_aNS.

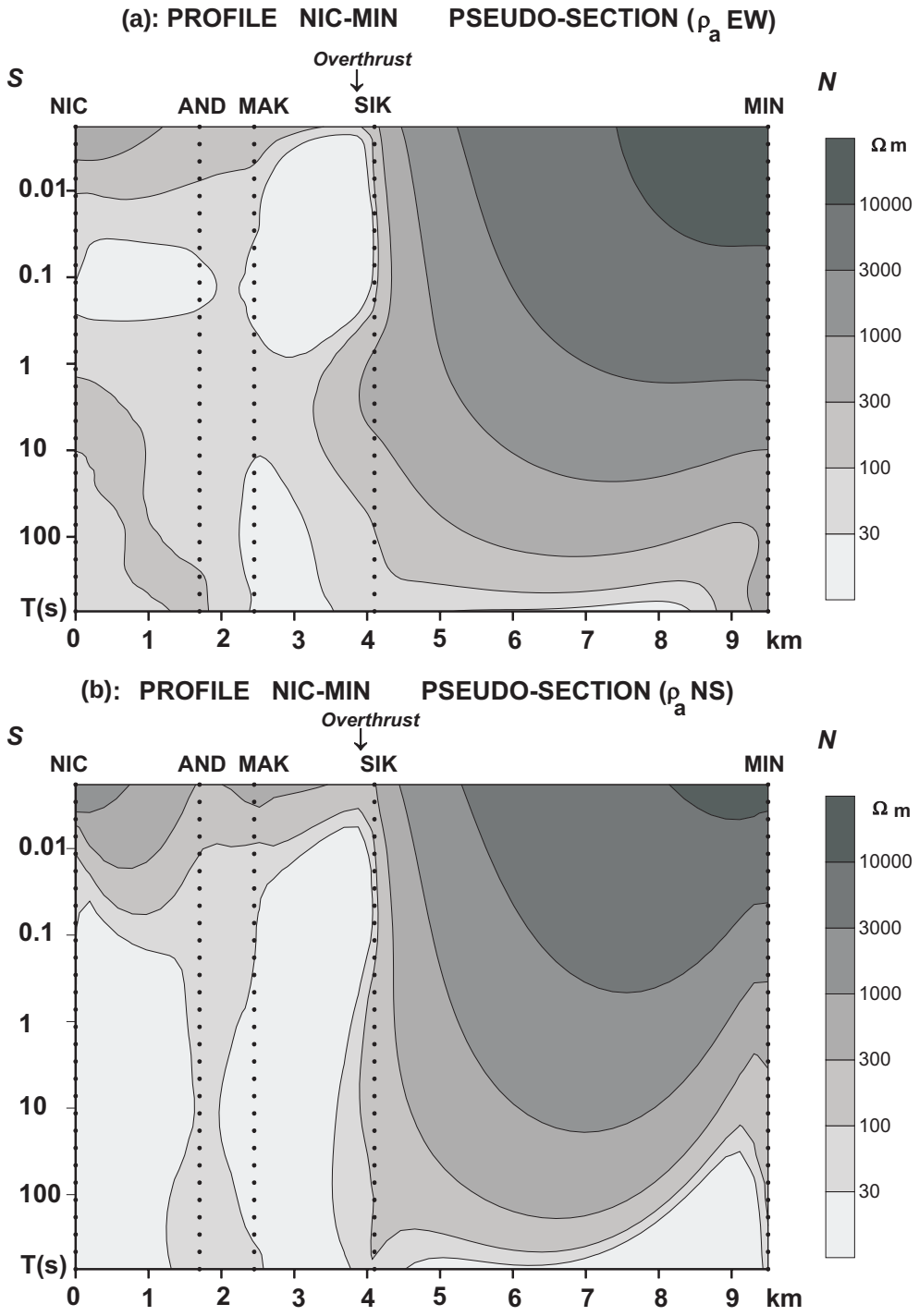

Figure 16. Pseudo-sections of the profile NIC-MIN (DD′ in Fig. 1). (a) ρ_aEW; (b) ρ_aNS.

overthrusting of allochthonous nappes on to the autochthonous basement along the ductile Phyllite series, which may be considered as a flat shear zone located at the base of the nappes. The presence of fluid-filled cracks in this shear zone contributes to a lower bulk resistivity. This phenomenon has been widely observed and verified by high-precision vertical seismic reflection investigations in several orogens. Large-scale overthrusting in the upper crust and detachment of the lower crust were identified in these sites by the presence of layering of the seismic reflectors associated with a conductive layer (Pham *et al.* 1990, 1998; Jones 1992, 1998).

As discussed above, the Phyllite series seems to be the best candidate in explaining the origin of the conductive layer in the middle crust. It is important to note that the 'geoelectrical section' differs from the 'geological section' in that boundaries between layers are determined by resistivity contrasts rather than by a combination of geological parameters. The resistivity depends not only on the lithology, but also on the porosity and fluid content, so that the conductive shear zone may be thicker than the Phyllite series. For the same reason, the resistivity of the conductive layer is not constant over the study area, as observed for the different profiles described in Section 6.

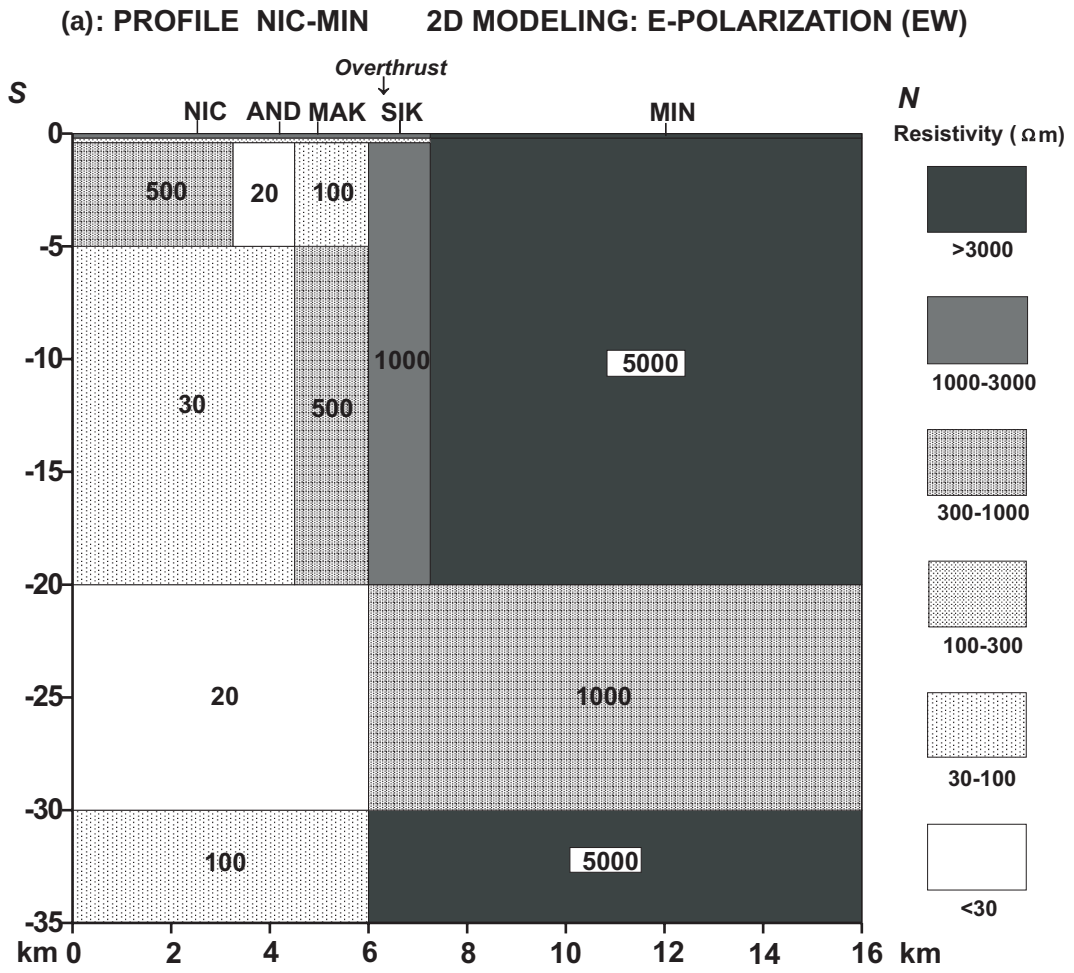

Figures 17. 2-D geoelectrical sections of the profile NIC-MIN. (a) *E*-polarization mode; (b) *H*-polarization mode.

8 CHARACTERISTICS OF THE ELECTRICAL ANISOTROPY OF THE CRUST

These characteristics have been described in detail in Sections 4, 5 and 6. The overall results indicate the anisotropic nature of the crust under the study area around the Gulf of Corinth. There exist two principal anisotropy directions, trending approximately E–W and N–S, parallel to the strike of the Corinth rift and to the strike of the Hellenides range, respectively. In the upper crust of some areas the anisotropy characteristics are more complex, presumably because of the superposition of these two structures.

Electrical images, in the form of apparent resistivity maps (Section 5) and 1-D or 2-D geoelectrical sections (Section 6), show the existence of a resistive and anisotropic upper crust, especially under the Parnassos zone, which consists predominantly of carbonates. This anisotropy is of intrinsic type, resulting from the E–W compression of the Hellenides, which leads to a more conductive axis along the N–S direction (macro- or microanisotropy). In some areas such as in the zones of E–W normal faulting related to N–S extension of the Gulf and in the front of the overthrust, a more complex apparent anisotropy resulting from the heterogeneity of the structure can be interpreted only from 2-D modelling. Models reveal the deep structure of the fault zones, rooting at different depths in the upper crust. The Helike fault, on the southern side of the Gulf, and the fault system in the Psaromita peninsula introduce anisotropy only in a shallow zone a few kilometres thick. On the other hand, the Mamousia fault, the overthrust of the Transition zone over the Pindos zone and the fault system in the Pangalos peninsula introduce more important anisotropy, affecting the whole upper crust above the middle conductive layer.

Finally, a more complicated electrical anisotropy feature is observed on the apparent resistivity maps in the Sotaina area, where the structure is probably 3-D. Its origin is unknown, but a connection with a major bend in the overthrust of the Transition zone over the Pindos zone seems plausible. As shown in the 2-D model of the PSA-AMI profile (Fig. 11), this overthrust roots deeply in the crust, consistent with the report of many outcrops of spilite and peridotite bodies on its front around the Sotaina area (from the 1:50 000 geological map of Greece, Amygdalea sheet).

The short-wavelength Sotaina anomaly is superimposed on the larger-scale electrical features discussed previously. In order to assess the existence and significance of this anomaly—to make it clear that it is not a residual effect of the contouring—we give in Appendix A an elementary 3-D modelling of the structure.

9 DISCUSSION AND CONCLUSIONS

The electrical results presented in this paper contribute to a better understanding of the deep structure of the upper crust and of its relationship with the seismotectonics around the Gulf of Corinth.

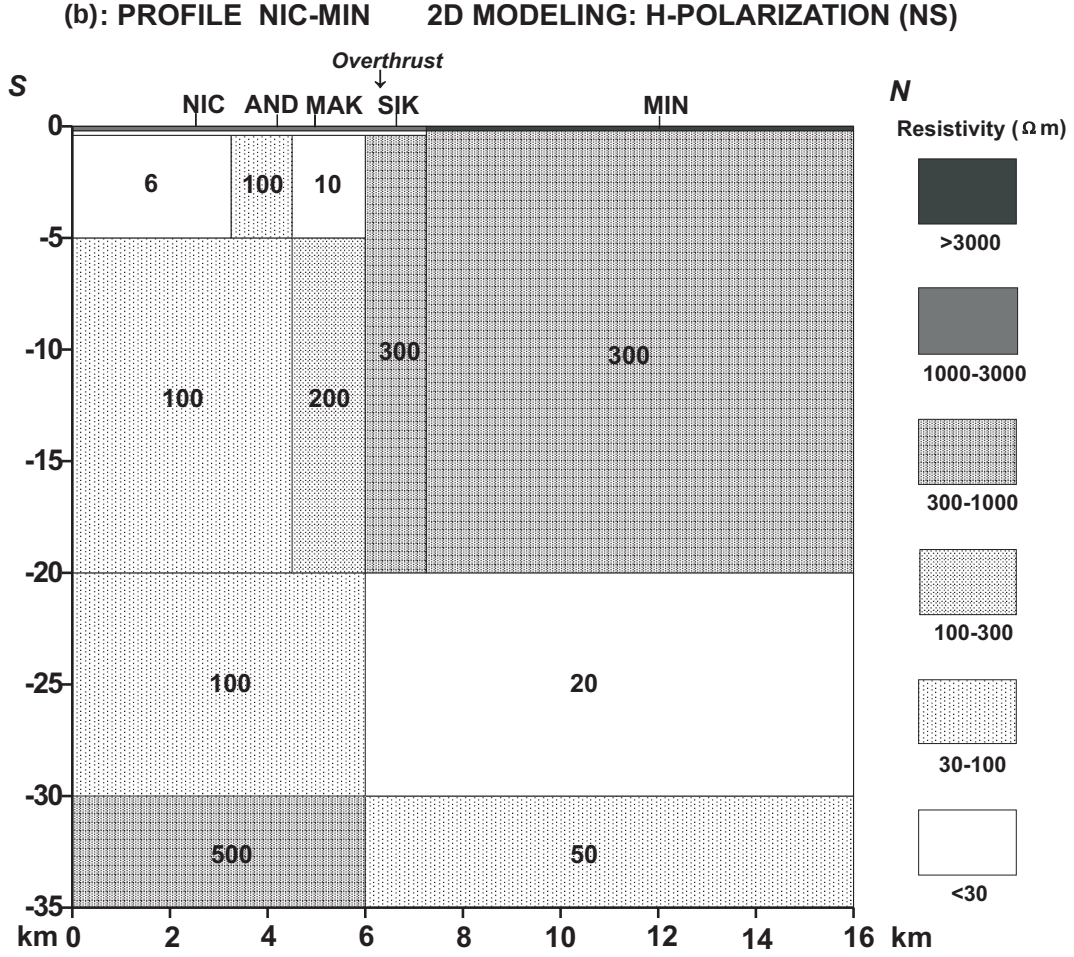

Figure 17. (*Continued.*)

Seismic and microseismic studies in the Gulf of Corinth have pointed out the seismotectonic significance of the geometry and kinematics of large-scale normal active faults (King *et al.* 1985; Doutsos & Poulimenos 1992; Rigo *et al.* 1996). However, the geometry of these normal faults is well known only at the ground surface, thanks to detailed geological mapping (Armijo *et al.* 1996), except for the results from a recent multidisciplinary study, which indicate low-angle normal faulting at 10 km depth related to the $Ms = 6.2$ 1995 June 15 Aigion earthquake (Bernard *et al.* 1997a). The extent of the normal faults in the deep crust and the existence of the detachment zone were until now highly speculative.

The study of the electrical properties of the crust in the western part of the study area confirms the existence of a relatively conductive layer in the middle crust that may be considered as a ductile layer because of the presence of fluids. This conductive layer is not confined to the centre of the rift, contrary to the hypothesis of a detachment zone by Rigo *et al.* (1996), and is thus probably inherited from the past thrust tectonics of the Hellenides. We propose that it results from the presence of a highly deformable Phyllite series.

This highly conductive layer is absent at mid-crustal depths in the eastern part of the study area (NIC-MIN profile), suggesting that the ductile crust is at a greater depth, possibly below 20 km. This interpretation of the difference between the eastern and western electrical structures is consistent with the characteristics of the microseismicity of the rift and with the global strain rate pattern deduced from GPS data. Indeed, the latter shows that the N–S extension strain rate in the western part is of the order of 1.5×10^{-6} yr^{-1}, whereas it is of the order of 0.5×10^{-6} yr^{-1} in the eastern part (Briole *et al.* 1999). We suggest that the thinner elastic crust in the western part results, for a given loading stress, in a higher strain rate than in the eastern part, where the elastic crust is thicker. The seismicity is in agreement with such a model. Although the large earthquakes are equally distributed along the whole rift (Papazachos & Papazachos 1997), the present microseismic activity is much higher in the western part of the rift, the eastern limit of this active region being the western shore of Itea bay (Fig. 18).

Concerning the deep structure of the central Hellenides, there is some evidence that the overthrust of both the Parnassos zone and the Transition zone over the Pindos zone corresponds to a major fault zone that extends at least down to the ductile zone (Fig. 13). Below this zone, at greater depths in the lower crust, the interpretation of the results is more ambiguous since the conductive layer acts as a screen for the penetration of the electromagnetic field.

The electrical image of the overthrust in the upper crust suggests that the central Hellenides are not composed of a stack of flat-lying nappes (Doutsos & Poulimenos 1992), as shown in Fig. 2, which is a very schematic cross-section through the nappe sequence. A more realistic geological image is a stack of thick folded nappes that displays the intrinsic anisotropy characteristics discussed in the preceding sections. The contact

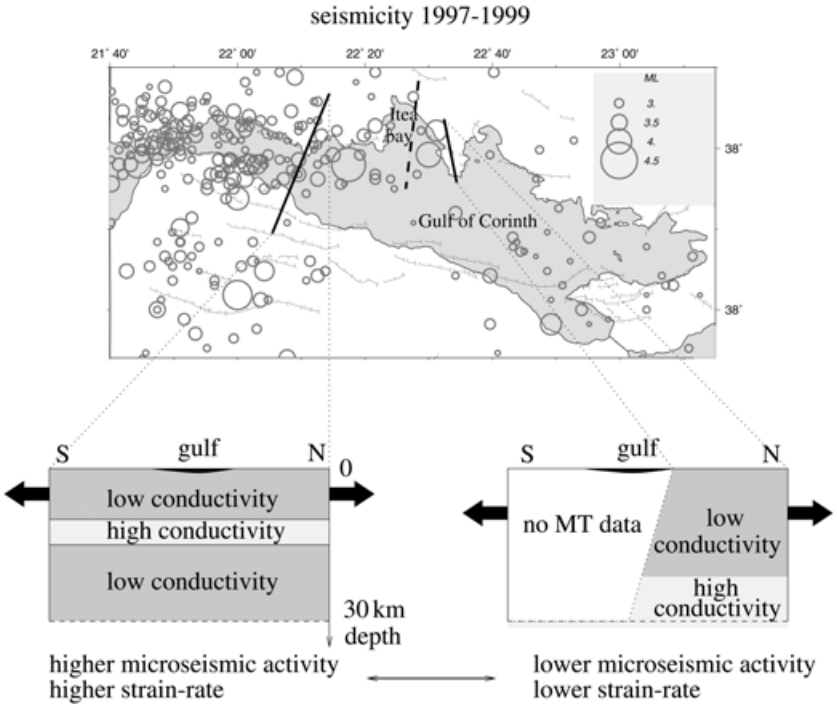

Figure 18. A possible model for the Corinth rift opening dynamics. Top: seismicity for the period January 1997–March 1999 (excluding the $M = 5.3$ Agios Pandes 1997 main shock–aftershock sequence), characteristic of the well-recorded activity since 1964 (National Observatory of Athens catalogue). Thick segments are the MT profiles. Dashed segment is the approximate location of the eastern boundary of the mid-crustal conductive layer. Bottom left: N–S vertical cross-section corresponding to the western profiles. The elastic loading is concentrated above the conductive layer, which is assumed to relax stress significantly, resulting in the observed high strain rate and microseismicity. Bottom right: N–S vertical cross-section corresponding to the eastern profile and its southern elongation without MT data. The elastic loading is distributed in a thicker elastic crust, resulting in lower strain rate and lower microseismicity.

between the nappes of the sequence is not flat, but probably subvertical. More generally, the electrical properties of the isopic zones depend not only on their lithology but also on the tectonics-related strain.

Concerning the normal fault striking E–W on the southern side of the Gulf, the electrical image of the Mamousia fault (Fig. 10) is consistent with the presence of a large curved ramp in the upper crust defining a major listric fault zone that is connected to the middle conductive ductile layer, which is expected to favour the detachment of the upper crust and the rifting. The Helike fault is also expected to root in this layer at depth. The absence of an electrical signature of this fault in the upper crust contrasts with the low resistivity of the Mamousia fault, implying that the latter is associated with more intense fracturing.

The electrical anisotropy affecting shallow heterogeneous zones or deep crustal structures has been thoroughly examined, providing information complementary to seismic anisotropy studies (Bouin *et al*. 1996) performed in order to investigate the stress field and its temporal variation in relation to the short- and long-term tectonic activity of fault systems (Gamar *et al*. 1999).

Finally, the overall electrical results will contribute to a better choice of sites for further monitoring of possible electromagnetic and self-potential signals that could be related to the seismic activity of the Gulf (the European GAIA programme and the French microsatellite DEMETER programme). Indeed, under the working hypothesis that conductive anomalous structures cutting through the brittle crust may allow the amplification of mid-crustal electrical sources in relation to seismic or aseismic slip (Bernard & Le Mouël 1996), a possible site is the anomalous Sotaina area, where the apparent resistivity is as low as a few ohm metres (see Appendix A). Other interesting sites are the Mamousia fault zone, the Psaromita peninsula and the Pangalos peninsula, where the electric results show evidence of a strong, deeply rooted fractured zone related to the recent tectonic activity.

ACKNOWLEDGMENTS

This work was supported by the programme 'DBT Fluides dans la croûte' of the INSU-CNRS (France), the CE Environment Programme, Topic Seismic Risk (contract ENV4-CT96–0276), the GAIA Project and the Laboratoire de Géomagnétisme of the IPGP. Special thanks are due to the technicians of the NOA who contributed to the fieldwork.

REFERENCES

Armijo, R., Meyer, B., King, G.C.P., Rigo, A. & Papanastassiou, D., 1996. Quaternary evolution of the Corinth Rift and its implication for the late Cenozoic evolution of the Aegean, *Geophys. J. Int.,* **126,** 11–53.

Aubouin, J., 1965. *Geosynclines,* Elsevier, Amsterdam.

Aubouin, J., Brunn, J.H., Celet, P., Dercourt, J., Godfriaux, I. & Mercier, J.L., 1962. Esquisse de la géologie de la Grèce, *Mém. Hors Sér. Soc. Géol. France,* **2,** 583–610.

Bernard, P. & Le Mouël, J.L., 1996. On electrotelluric signals, in *A Critical Review of VAN*, pp. 118–152, ed. Lighthill, J., World Scientific, Singapore.

Bernard, P. *et al.*, 1997a. The Ms = 6.2, June 15, 1995 Aigion earthquake (Greece): evidence for low angle normal faulting in the Corinth rift, *J. Seism.,* **1,** 131–150.

Bernard, P., Chouliaras, G., Tzanis, A., Bride, P., Bouin, M.P., Tellez, J., Stavrakakis, G. & Makropoulos, K., 1997b. Seismic and electrical anisotropy in the Mornos delta, Gulf of Corinth, Greece, and its relationship with GPS strain measurements, *Geophys. Res. Lett.,* **24,** 2227–2230.

Bouin, M.P., Tellez, J. & Bernard, P., 1996. Seismic anisotropy around the Gulf of Corinth, Greece, deduced from three-component seismograms of local earthquakes and its relationship with crustal strain, *J. geophys. Res.,* **101,** 5797–5811.

Briole, P. *et al.*, 1999. Active deformation of the Gulf of Corinth, Greece: results from repeated GPS surveys between 1990 and 1995, *J. geophys. Res.,* in press.

Cagniard, L., 1953. Basic theory of magnetotelluric method of geophysical prospecting, *Geophysics,* **18,** 605–635.

Chouliaras, G., Pham, V.N., Boyer, D., Bernard, P. & Stavrakakis, G.N., 1997. Crustal structure of the Gulf of Corinth in Central Greece, determined from magnetotelluric soundings, *Ann. Geofis.,* **40,** 61–67.

Doucet, D. & Pham, V.N., 1984. Généralisation et optimalisation de la méthode des différences finies pour la modélisation en magnétotellurique, *Geophys. Prospect.,* **32,** 303–314.

Doutsos, T. & Poulimenos, G., 1992. Geometry and kinematics of active faults and their seismotectonic significance in the western Corinth-Patras rift (Greece), *J. struct. Geol.,* **14,** 689–699.

Gamar, F., Bernard, P., Pham, V.N., Boyer, D., Papadimitriou, P., Chouliaras, G. & Charrier, A., 1999. Spatial and temporal variation of seismic and electric anisotropy and its relationship with crustal strain in the Psaromita peninsula, Gulf of Corinth, Greece, *J. geophys. Res.,* submitted.

Jacobshagen, V., Richter, D. & Makris, J., 1978a. Alpidic development and structure of the Peloponnesus, in *Alps, Apennines, Hellenides,* pp. 415–423, eds Closs, H., Roeder, D. & Schmidt, K., Schweiz-Verlag, Stuttgart.

Jacobshagen, V., Dürr, S.t., Kockel, F., Kopp, K.O. & Kowalczyk, G., 1978b. Structure and geodynamic evolution of the Aegean region, in *Alps, Appennines, Hellenides,* pp. 537–564, eds Closs, H., Roeder, D. & Schmidt, K., Schweiz-Verlag, Stuttgart.

Jones, A.G., 1992. Electrical properties of the lower continental crust, in *Continental Lower Crust,* pp. 81–131, eds Fountain, D.M., *et al.*, Elsevier, Amsterdam.

Jones, A.G., 1998. Waves of the future: superior inferences from collocated seismic and electromagnetic experiments, *Tectonophysics,* **286,** 273–298.

Keller, G.V. & Frischknecht, F.C., 1966. *Electrical Methods in Geophysical Prospecting,* Pergamon, Oxford.

King, G.C.P. *et al.*, 1985. The evolution of the Gulf of Corinth (Greece): an aftershock study of the 1981 earthquakes, *Geophys. J. R. astr. Soc.,* **80,** 677–683.

Lyon-Caen, H. *et al.*, 1988. The 1986 Kalamata (South Peloponnesus) earthquake: detailed study of a normal fault, evidence for east–west extension in the Hellenic arc, *J. geophys. Res.,* **93,** 14 967–15 000.

Makris, J., 1978. The crust and upper mantle of the Aegean region from deep seismic soundings, *Tectonophysics,* **46,** 269–284.

Melis, N.S., Brooks, M. & Pearce, R.G., 1989. A microearthquake study in the Gulf of Patras region, western Greece, and its seismotectonic interpretation, *Geophys. J. R. astr. Soc.,* **98,** 515–524.

Ori, G.G., 1989. Geologic history of the extensional basin of the Gulf of Corinth (? Miocene–Pleistocene), Greece, *Geology,* **17,** 918–921.

Papazachos, B.C. & Papazachos, C.B., 1997. *The Earthquakes of Greece,* Ziti Publications, Thessaloniki.

Pham, V.N., Boyer, D. & Cazes, M., 1990. Deep seismic and magnetotelluric sounding in Northern France, in *The Potential of Deep Seismic Profiling for Hydrocarbon Exploration,* pp. 105–116, eds Pinet, B. & Bois, C., Technip, Paris.

Pham, V.N., Boyer, D., Chouliaras, G. & Bernard, P., 1996. Electrical conductivity and structure of the crust around the Gulf of Corinth (Greece) from magnetotelluric sounding (MTS) results, *C. R. Acad. Sci. Paris,* **323,** 651–656.

Pham, V.N., Boyer, D. & Mattauer, M., 1998. Electrical properties and structure of the earth's crust under the northern part of the Ecors-Pyrénées profile from magnetotelluric sounding results, *Mem. Soc. géol. France,* **173,** 83–90.

Rigo, A., Lyon-Caen, H., Armijo, R., Deschamps, A., Hatzfeld, D., Makropoulos, K., Papadimitriou, P. & Kassaras, I., 1996. A microseismic study in the Western part of the Gulf of Corinth (Greece): implications for large-scale normal faulting mechanisms, *Geophys. J. Int.,* **126,** 663–688.

Ting, S.C. & Hohmann, G.W., 1981. Integral equation modeling of three-dimensional magnetotelluric response, *Geophysics,* **46,** 182–197.

Vozoff, K., 1991. The magnetotelluric method, in *Electromagnetic Methods in Applied Geophysics,* pp. 641–711, ed. Nabighian, M.N., *SEG Investigations in Geophysics No. 3,* Vol. 2, SEG, Tulsa, OK.

APPENDIX A: TENTATIVE INTERPRETATION OF THE SOTAINA ANOMALY USING A 3-D MODEL

As indicated in Section 8, a complicated electrical anisotropy feature is observed on the apparent resistivity maps in the Sotaina area, where the deep structure is probably 3-D. An overall 3-D MT interpretation is still not practical because 3-D modelling routines require a high density of measured sites in the studied area to handle complex Earth structure. In the Sotaina area, six stations in close proximity to one another were occupied in order to try and confirm the existence of the local electrical anomaly, but their distribution is still sparse because the region is mountainous and hard to access. Nevertheless, we think this anomaly is real since we can observe it on all of the apparent resistivity maps corresponding to different frequencies (Figs 4, 5 and 6). Figs A1 (a) and (b) show more detailed maps of the Sotaina area corresponding, respectively, to ρ_aEW and ρ_aNS for another period, $T=10$ s. Again, a local anomalous conductive zone appears clearly, the image of which has the characteristics of a 3-D structure. The values of the apparent resistivity at each station confirm that the observed anomaly is not a residual effect of contouring. Moreover, station SO2, located inside the anomalous zone, in fact represents two stations (SO1 and SO2) that were located at the same site and show the same MTS results. The sparse distribution of the stations certainly does not allow one to define the exact shape of the structure. It is nevertheless possible to compare the observed electrical image with that provided by a simple 3-D model. Numerical results for three dimensions have been available since the 1980s (Vozoff 1991). The most interesting model is that of Ting & Hohmann (1981), showing the distribution of apparent resistivity around a simple 3-D body at a period $T=10$ s, which can be compared with the detailed Sotaina maps. The model is a 3-D conductive prism (5 Ωm) buried in a homogeneous resistive half-space earth (100 Ωm) (Fig. A2). From the Ting & Hohmann's (1981) numerical results, we have redrawn, using the same scale as in Fig. A1, two apparent resistivity maps corresponding to the two principal directions, E–W and N–S, for the period $T=10$ s (Figs A3a and b). Globally, the image of the anomaly on these maps is comparable with the image of the Sotaina maps (Fig. A1), with the same order of apparent resistivities. The shape of the anomaly is not exactly the same because the real geological structure is certainly more complex than a prismatic body. Moreover, the crust around the Sotaina area is inhomogeneous and strongly anisotropic, as explained above. We conclude that the Sotaina

anomaly can be attributed to the existence of a local conductive zone with approximately the characteristics of a 3-D body.

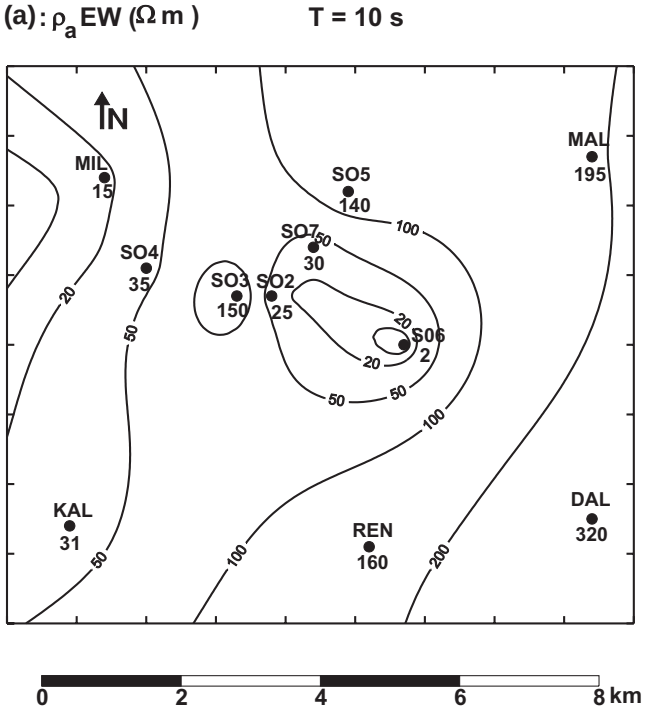

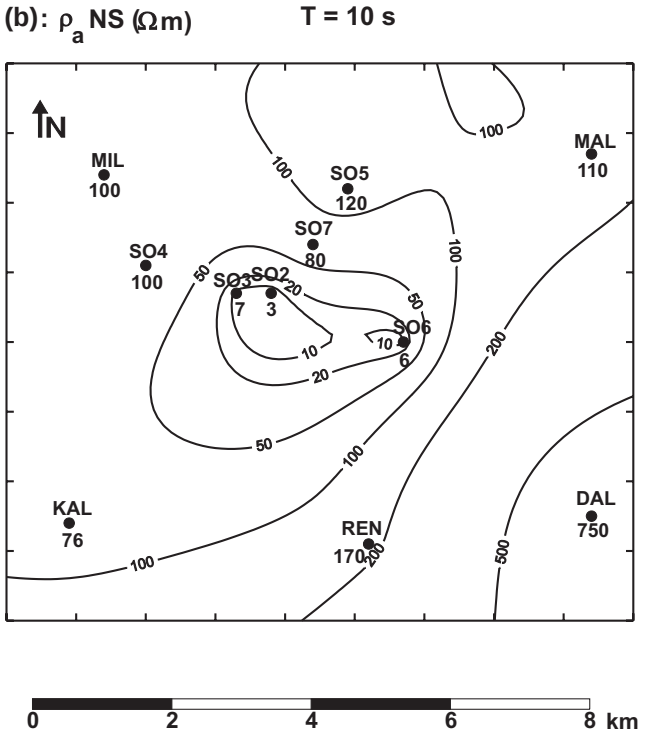

Figure A1. Detailed apparent resistivity maps of the Sotaina area for period $T = 10$ s for the two principal directions. (a) ρ_aEW; (b) ρ_aNS. Black circles: locations of the MTS stations with their names and values of apparent resistivity in Ωm.

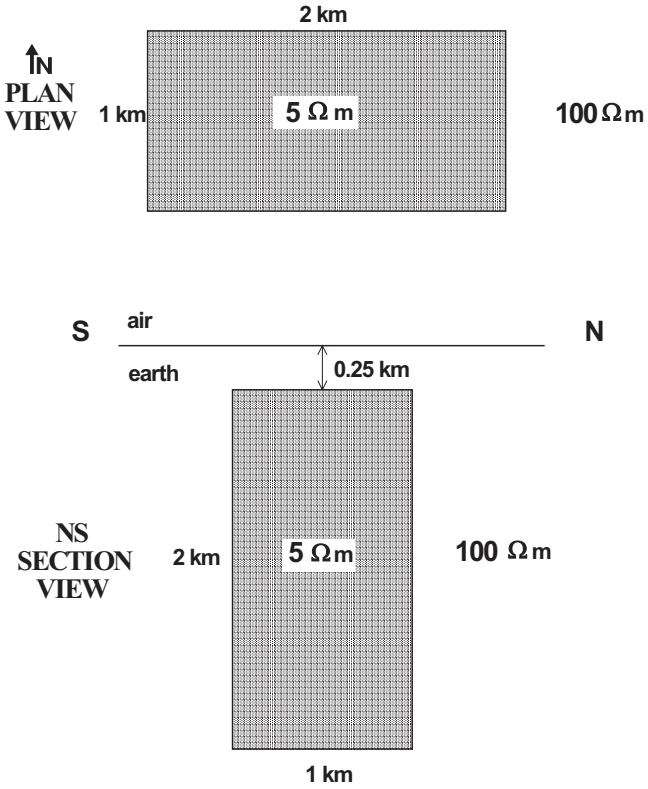

Figure A2. 3-D model used to calculate various MT parameters redrawn from Ting & Hohmann (1981).

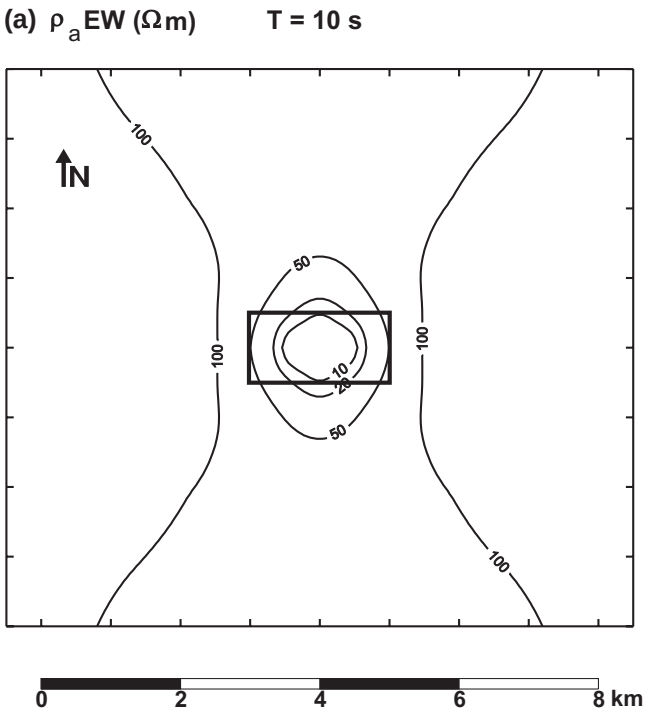

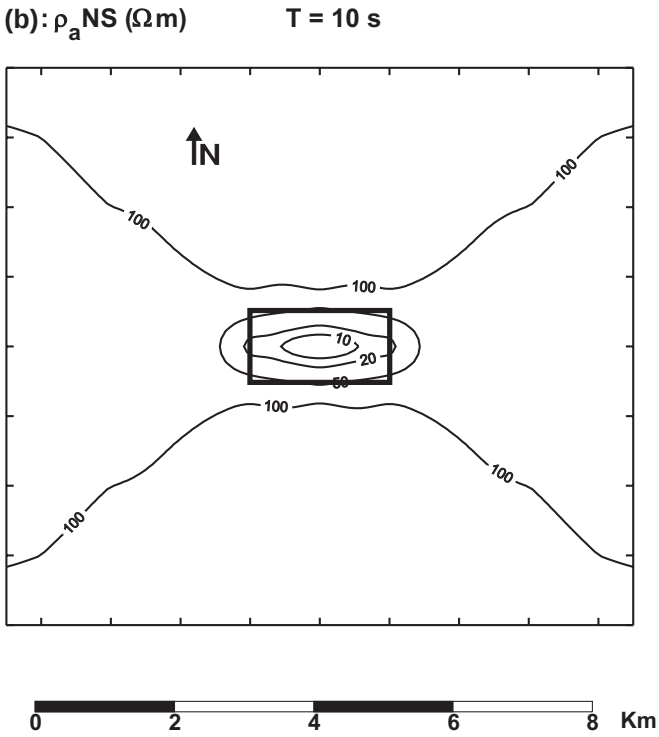

Figure A3. Apparent resistivity maps redrawn from Ting & Hohmann's (1981) numerical results for the model shown in Fig. A2 at a period $T = 10$ s for the two principal directions. (a) ρ_aEW; (b) ρ_aNS. Rectangular heavy black contour: plan view of the prismatic 3-D model.